Cell Insight 1 (2022) 100047

Contents lists available at ScienceDirect

Cell Insight

journal homepage: www.journals.elsevier.com/cell-insight

USP2 promotes experimental colitis and bacterial infections by inhibiting the proliferation of myeloid cells and remodeling the extracellular matrix network

Ran An [a,b,c], Peng Wang [a,b], Hao Guo [a,b], Tianzi Liuyu [b], Bo Zhong [a,b,c,**], Zhi-Dong Zhang [a,b,c,*]

[a] Department of Gastrointestinal Surgery, College of Life Sciences, Zhongnan Hospital of Wuhan University, Wuhan, 430071, China
[b] Department of Immunology, Medical Research Institute and Frontier Science Center for Immunology and Metabolism, Wuhan University, Wuhan, 430072, China
[c] Wuhan Research Center for Infectious Diseases and Cancer, Chinese Academy of Medical Sciences, Wuhan, 430071, China

HIGHLIGHTS

- Knockout of USP2 in myeloid cells suppresses DSS-induced colitis and bacterial infection.
- USP2 inhibits the proliferation of myeloid cells to suppress T cell activation in the colon.
- Knockout of USP2 in myeloid cells leads to ECM dysregulation and protects the integrity of gut epithelium.
- Pharmacological inhibition of USP2 alleviates DSS-induced colitis.

GRAPHICAL ABSTRACT

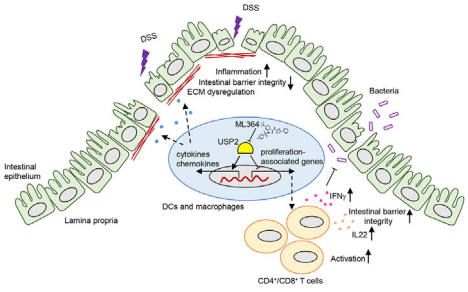

ARTICLE INFO

Keywords:
USP2
Colitis
Bacterial infection
Cell proliferation
Myeloid cells

ABSTRACT

Inflammatory bowel disease (IBD) is closely associated with dysregulation of genetic factors and microbial environment. Here, we report a susceptible role of ubiquitin-specific protease 2 (USP2) in experimental colitis and bacterial infections. USP2 is upregulated in the inflamed mucosa of IBD patients and in the colon of mice treated with dextran sulfate sodium salt (DSS). Knockout or pharmacologic inhibition of USP2 promotes the proliferation of myeloid cells to activate IL-22 and IFNγ production of T cells. In addition, knockout of USP2 in myeloid cells inhibits the production of pro-inflammatory cytokines to relieve the dysregulation of extracellular matrix (ECM) network and promote the gut epithelial integrity after DSS treatment. Consistently, *Lyz2*-Cre;*Usp2*$^{fl/fl}$ mice exhibit hyper-resistance to DSS-induced colitis and *Citrobacter rodentium* infections compared to *Usp2*$^{fl/fl}$ mice. These findings highlight an indispensable role of USP2 in myeloid cells to modulate T cell activation and epithelial ECM network and repair, indicating USP2 as a potential target for therapeutic intervention of IBD and bacterial infections in the gastrointestinal system.

1. Introduction

Inflammatory bowel disease (IBD), including ulcerative colitis (UC) and Crohn's disease (CD), is a multifactorial inflammatory disease of the colon and small intestine and becomes an increasing threat to human health worldwide (Xavier and Podolsky, 2007). While the pathogenesis of IBD is incompletely understood, emerging studies suggest that genetic and environmental factors can play an indispensable role (Cleynen et al.,

** Corresponding author. Department of Gastrointestinal Surgery, College of Life Sciences, Zhongnan Hospital of Wuhan University, Wuhan, 430071, China.
* Corresponding author.
E-mail addresses: zhongbo@whu.edu.cn (B. Zhong), zhidongzhang@whu.edu.cn (Z.-D. Zhang).

https://doi.org/10.1016/j.cellin.2022.100047
Received 19 April 2022; Received in revised form 21 June 2022; Accepted 4 July 2022
Available online 8 July 2022

2016; Yilmaz et al., 2019). Available studies have demonstrated dysregulation of gene expression profiles in the inflamed mucosa of IBD patients which facilitates or inhibits the progression of IBD. For example, mutation or deletion of NOD2 and IL-10 leads to IBD aggravation, while USP25 and TNFSF15 deficiency contributes to IBD attenuation (Glocker et al., 2009; Ogura et al., 2001; Wang et al., 2020; Yamazaki et al., 2005). Besides, multiple environmental factors that encompass pregnancy, mode of birth, and lifestyle exposures during childhood and adulthood have been related to the development of IBD (Ananthakrishnan et al., 2018). The intestinal microbiota has been reported to regulate immune factors, repair intestinal barrier function, and maintain intestinal environmental homeostasis (Shamoon et al., 2019). Uncertain environmental factors can disrupt intestinal homeostasis and lead to intestinal inflammation, which further alters the component and function of intestinal microbiota (Li et al., 2016). Studies have shown that IBD patients have a decreased intestinal microbiota abundance with the increase of aggressive species such as *Fusobacterium* and the decrease of protective species compared with healthy individuals (Shah et al., 2016).

Intestinal myeloid cells could trigger innate immune responses against the invading pathogenic microorganisms through pattern-recognition receptors (PRRs) that detect microbial pathogen-associated molecular patterns (PAMPs) (Akira et al., 2006). The myeloid cells serve as antigen-presenting cells (APCs) to activate T cells by upregulating the MHC molecules and costimulatory signals which promotes adaptive immunity in a manner of activation, differentiation and expansion of T cells (Ben-Sasson et al., 2009; Gerner et al., 2013; Roche and Furuta, 2015). In addition, myeloid cells such as monocytes and macrophages are also involved in tissue homeostasis and injury repair (van Amerongen et al., 2007). In IBD, myeloid cells secrete growth factors, proteolytic enzymes, angiogenic factors, and fibrogenic cytokines to remodel the extracellular matrix (ECM) including collagen and fibronectin, which finally contributes to intestinal epithelial repair and regeneration (Ogle et al., 2016). Intestinal ECM provides physical support for intestinal integrity and elasticity and is a dynamic structure constantly remodeled to maintain intestinal homeostasis (Bonnans et al., 2014). However, chronic or severe tissue injuries caused by pathogen-mediated inflammatory responses could promote excessive production and deposition of ECM, which finally leads to intestinal fibrosis of IBD and exacerbates inflammation (Lawrance et al., 2017; Wang et al., 2021).

Migration and proliferation of cells is vital for the development and the homeostasis of tissues (Lautenschlager et al., 2009). During tissue damage and inflammation, circulating myeloid cells migrate to sites of infection and injury and self-proliferate, subsequently initiating immune responses. Such a process of migration is dependent on specific molecular markers expressed on the cell surface such as integrins and chemokine receptors (Neurath, 2019). For example, CCR2, MCP-1, and MCP-3 deficient monocytes could not emigrate out of bone marrow in thioglycolate-induced peritonitis (Tsou et al., 2007). Moreover, tissue-resident monocytes retain the capacity to proliferate in response to inflammatory stimuli in many diseases such as liver injury, heart disease, insulitis, atherosclerosis, and kidney injury (Andres et al., 2012; Hulsmans et al., 2016; Tacke and Zimmermann, 2014; Wen et al., 2021; Ying et al., 2020).

USP2 is a member of the ubiquitin-specific protease (USP) family, which is expressed in multiple organs including the testis, heart, liver, brain, and kidney (Kitamura and Hashimoto, 2021). In recent decades, a critical role of USP2 has been suggested in inflammatory responses and tumorigenesis (Kitamura and Hashimoto, 2021). We previously reported that USP2 facilities tumor metastasis through tuning TGF-β-triggered signaling (Zhao et al., 2018). However, where its role in bacterial infections, infection-associated, or chemically induced colitis is unclear. Here, we report that USP2 deficiency in myeloid cells leads to hyper-immune responses after dextran sulfate sodium (DSS) treatment or *Citrobacter rodentium* infection. We further found that USP2 inhibits the proliferation of myeloid cells to suppress the activation and expansion of $CD4^+$ T cells and $CD8^+$ T cells and the production of IL-22 and IFNγ. Moreover, knockout of USP2 in myeloid cells impaired the production of inflammatory factors and altered the extracellular matrix in the inflamed colon. Finally, pharmacological inhibition of USP2 could alleviate colitis and promotes gut epithelial repair after DSS treatment. These findings collectively suggest that USP2 plays a critical role in colitis and may serve as a potential therapeutic target.

2. Results

2.1. USP2 plays a pro-inflammatory role in DSS-induced colitis

Because inflammatory bowel disease (IBD) is associated with dysregulation of gene expression profile (Cleynen et al., 2016), we hypothesized that the aberrantly expressed genes in the inflamed colon tissues of IBD patients might play roles in IBD progression. Analyses of the transcriptomic data of the colon tissues from patients with ulcerative colitis (UC) led to the identification of USP2 as a highly expressed gene in the inflamed tissues compared to the healthy colon mucosa (Fig. 1A). Further analyses of the single-cell transcriptome data suggested that USP2 was highly expressed in the epithelium and the myeloid cells such as macrophages, dendritic cells and monocytes but not in the lymphocytes of the inflamed mucosa (Smillie et al., 2019) (Fig. S1A). These data were in agreement with our observations that murine *Usp2* was detected in both the intestinal epithelial cells (IECs) and the lamina propria mononuclear cells (LPMCs) in the colon and was upregulated in LPMCs after dextran sulfate sodium (DSS) challenge (Figs. S1B and S1C). These data suggest that USP2 is upregulated in the inflamed colon tissues in DSS-treated mice and in UC patients.

We next investigated the roles of USP2 in DSS-induced colitis in mice. The $Usp2^{+/+}$ and $Usp2^{-/-}$ mice were fed with 3% DSS for 5 successive days and then with normal sterile water for 3 days (Wang et al., 2020; Zhao et al., 2018). We found that the $Usp2^{-/-}$ mice were more resistant to weight loss than the $Usp2^{+/+}$ mice after DSS treatment (Fig. 1B). Consistently, the $Usp2^{-/-}$ mice exhibited longer colons, lower pathology scores and milder colon ulcers than the $Usp2^{+/+}$ mice (Fig. 1C and D), indicating a pro-inflammatory role of USP2 in DSS-induced colitis.

2.2. Knockout of USP2 in myeloid cells alleviates DSS-induced colitis

To further characterize the cellular source of USP2 that contributed to DSS-induced colitis, we generated $Usp2^{fl/fl}$ mice with exons 4–6 flanked by loxp sites through CRISPR/Cas9-mediated genome editing (Fig. S1D). Results from Southern blot analysis suggested that the targeting vector was correctly recombined into the *Usp2* genome (Fig. S1E). Cre recombinase-mediated deletion of exons 4–6 would result in mRNA instability or early termination of mRNA translation (Fig. S1F). We next examined the roles of USP2 in gut epithelial cells and T cells during colitis. We obtained *Vil*-Cre;$Usp2^{fl/fl}$ mice by crossing the $Usp2^{fl/fl}$ mice with the *Vil*-Cre mice (Wang et al., 2020). Results from qRT-PCR analysis suggested that the mRNA levels of *Usp2* were substantially reduced in the colonic epithelial cells (ECs) of *Vil*-Cre;$Usp2^{fl/fl}$ mice compared to those of $Usp2^{fl/fl}$ mice (Fig. S1G). However, the *Vil*-Cre;$Usp2^{fl/fl}$ mice exhibited similar weight loss compared to the $Usp2^{fl/fl}$ mice during colitis induction (Fig. S1H). Consistently, the colon length, pathology scores and the colonic ulcers were comparable between the *Vil*-Cre;$Usp2^{fl/fl}$ mice and the $Usp2^{fl/fl}$ mice (Fig. S1I and S1J). We also obtained CD4-Cre;$Usp2^{fl/fl}$ mice by crossing the $Usp2^{fl/fl}$ mice and the CD4-Cre mice and found that the mRNA levels of *Usp2* were almost abolished in $CD4^+$ T cells from CD4-Cre;$Usp2^{fl/fl}$ mice compared to those from $Usp2^{fl/fl}$ mice (Fig. S1K) (Wu et al., 2020). We induced colitis in these mice by feeding the mice with 3% DSS for 5 d followed by normal sterile water for 3 d and observed that the CD4-Cre;$Usp2^{fl/fl}$ mice exhibited similar weight loss compared to the $Usp2^{fl/fl}$ mice during colitis induction (Fig. S1L). In addition, the colon length, pathology scores and the colonic ulcers were comparable between t the CD4-Cre;$Usp2^{fl/fl}$ mice and the $Usp2^{fl/fl}$ mice

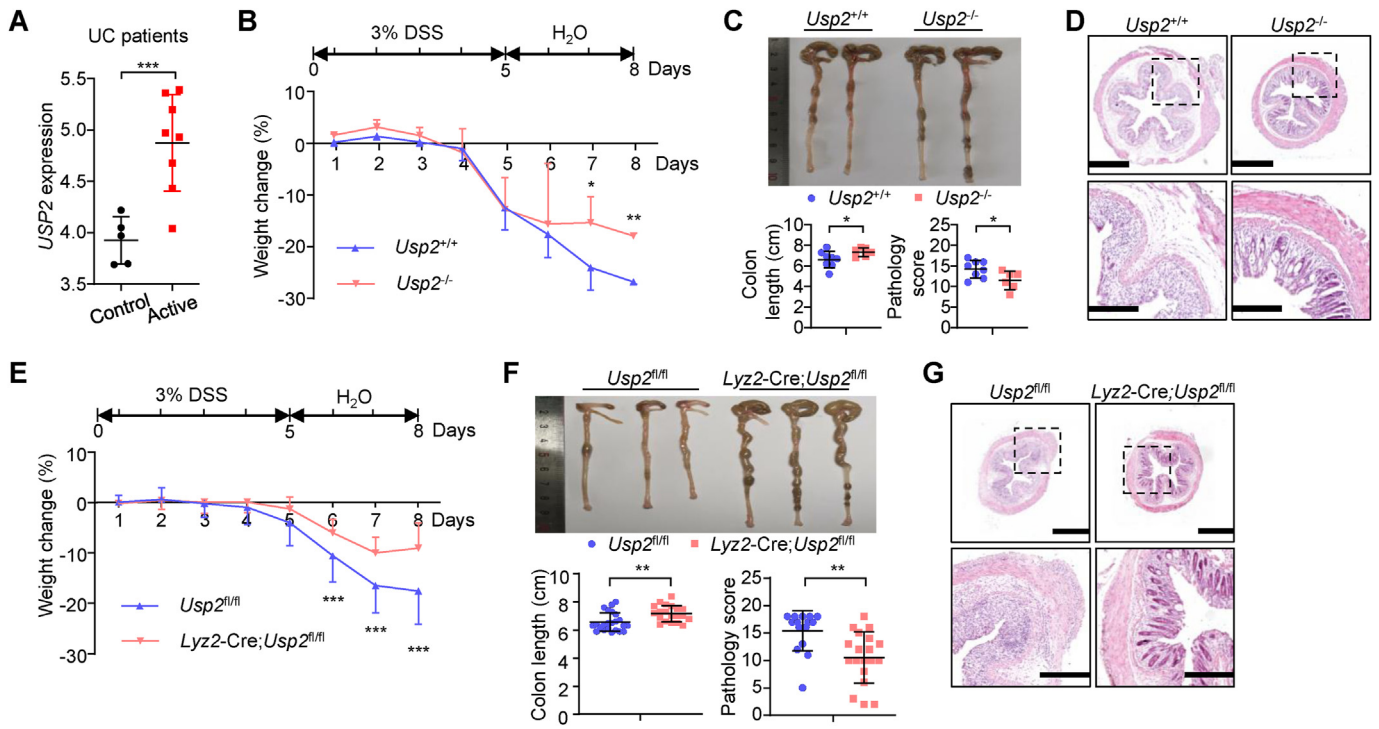

Fig. 1. USP2 plays a pro-inflammatory role in DSS-induced colitis.

(A) **USP2** mRNA expression level in colonic mucosa tissues from active ulcerative colitis (UC) patients and healthy people, the data were collected from GEO database (GDS3119) (n = 13).

(B) A scheme of DSS treatment and body weight change of $Usp2^{+/+}$ (n = 3) and $Usp2^{-/-}$ (n = 3) mice with DSS-induced colitis.

(C) The representative image and lengths of colons and pathology scores of $Usp2^{+/+}$ (n = 8) and $Usp2^{-/-}$ (n = 6) mice with DSS-induced colitis.

(D) HE-stained images of colon sections of $Usp2^{+/+}$ and $Usp2^{-/-}$ mice with DSS-induced colitis.

(E) A scheme of DSS treatment and body weight change of $Usp2^{fl/fl}$ (n = 24) and *Lyz2*-Cre;$Usp2^{fl/fl}$ (n = 24) mice with DSS-induced colitis.

(F) The representative image and lengths of colons and pathology scores of $Usp2^{fl/fl}$ (n = 24; 15) and *Lyz2*-Cre;$Usp2^{fl/fl}$ (n = 24; 19) mice with DSS-induced colitis.

(G) HE-stained images of colon sections of $Usp2^{fl/fl}$ and *Lyz2*-Cre;$Usp2^{fl/fl}$ mice with DSS-induced colitis.

$^{*}P < 0.05$, $^{**}P < 0.01$, $^{***}P < 0.001$ (Student's unpaired *t*-test). Scale bars represent 600 μm and 200 μm. Graphs show mean ± S.D. (A-C, E-F). Data are representative of two (B–D) independent experiments or a combination of four (E–G) independent experiments.

(Fig. S1M and S1N). These data indicate that USP2 in the epithelium or in T cells is dispensable for its pro-inflammatory role in the DSS-induced colitis model.

We further crossed the $Usp2^{fl/fl}$ mice with *Lyz2*-Cre mice to obtain the *Lyz2*-Cre;$Usp2^{fl/fl}$ mice (Liuyu et al., 2019). Results from flow cytometry analysis suggested that the proportions and the numbers of various lymphocytes and myeloid cells in thymus, spleen and inguinal lymph nodes were comparable between the *Lyz2*-Cre;$Usp2^{fl/fl}$ and the $Usp2^{fl/fl}$ mice (Fig. S2), suggesting an dispensable role of USP2 in the development and homeostasis of immune cells. We next induced colitis in these mice with DSS and monitored the weight loss (Fig. 1E), and found that the *Lyz2*-Cre;$Usp2^{fl/fl}$ mice were more resistant to weight loss and exhibited longer colon length and lower pathology scores than the $Usp2^{fl/fl}$ mice (Fig. 1E and F). Results from HE staining suggested that the colonic ulcers were milder in the *Lyz2*-Cre;$Usp2^{fl/fl}$ mice than in the $Usp2^{fl/fl}$ mice (Fig. 1G). Collectively, these data suggest that USP2 in myeloid cells promotes colon inflammation after DSS treatment.

2.3. Knockout of USP2 alters gene expression profile in myeloid cells after DSS treatment

To further explore the mechanism of USP2 in promoting DSS-induced colitis, we would like to analyze the gene expression profile in USP2-deficient and sufficient myeloid cells in the lamina propria after DSS treatment. To do this, we crossed *Lyz2*-Cre mice or *Lyz2*-Cre;$Usp2^{fl/fl}$ mice with the B6.Cg-Gt(ROSA)26Sor$^{tm14(CAG-tdTomato)Hze}$ fate-tracing mice (here referred to $Ai14^{LSL-TdTomato}$) to obtain the *Lyz2*-Cre;$Ai14^{LSL-TdTomato}$ and the *Lyz2*-Cre;$Usp2^{fl/fl}Ai14^{LSL-TdTomato}$ mice, respectively (Li et al., 2020). In these mice, Cre-mediated genome recombination removed the STOP cassette to allow the expression of tdTomato reporter in myeloid cells. As expected, all the RFP^{+} cells were found in the $CD45.2^{+}$ populations and consisted of $CD11b^{+}$ and $CD11c^{+}$ populations in the LPMCs under homeostatic conditions or after DSS treatment (Fig. 2A and Fig. S3A), and vice versa, most of the $CD11b^{+}$ and $CD11c^{+}$ populations (>80%) in the LPMCs expressed RFP (Fig. S3B). DSS treatment increased the numbers and percentages of RFP^{+} cells in the $CD45.2^{+}$ LPMCs of the *Lyz2*-Cre;$Ai14^{LSL-TdTomato}$ and the *Lyz2*-Cre;$Usp2^{fl/fl}Ai14^{LSL-TdTomato}$ mice (Fig. 2A). In addition, the percentages and numbers of RFP^{+} cells in the $CD45.2^{+}$ LPMCs of *Lyz2*-Cre;$Usp2^{fl/fl}Ai14^{LSL-TdTomato}$ mice were significantly increased compared to those of *Lyz2*-Cre;$Ai14^{LSL-TdTomato}$ mice (Fig. 2A). These data together suggest that knockout of USP2 increases myeloid cells in the lamina propria of mice after DSS treatment.

We next sorted the RFP^{+} cells from the $CD45^{+}$ LPMCs of *Lyz2*-Cre;$Ai14^{LSL-TdTomato}$ and *Lyz2*-Cre;$Usp2^{fl/fl}Ai14^{LSL-TdTomato}$ mice that were induced colitis and performed transcriptome sequencing assays (Fig. 2A). The results suggested that the expression of 63 genes and 30 genes were significantly downregulated (Log2[fold change] < −1) and upregulated (Log2[fold change] > 1) in RFP^{+} *Lyz2*-Cre;$Usp2^{fl/fl}Ai14^{LSL-TdTomato}$ cells compared to RFP^{+} *Lyz2*-Cre;$Ai14^{LSL-TdTomato}$ cells, respectively (Fig. 2B). KEGG and GSEA analysis suggested that the cytokine-chemokine signaling pathways and NF-κB signaling pathway were downregulated and the cell cycle and DNA replication pathways were upregulated in the *Lyz2*-Cre;$Usp2^{fl/fl}Ai14^{LSL-TdTomato}$ RFP^{+} LPMCs compared to the *Lyz2*-Cre; $Ai14^{LSL-TdTomato}$ counterparts (Fig. 2C and D). Results from qRT-PCR assays further confirmed that the genes encoding

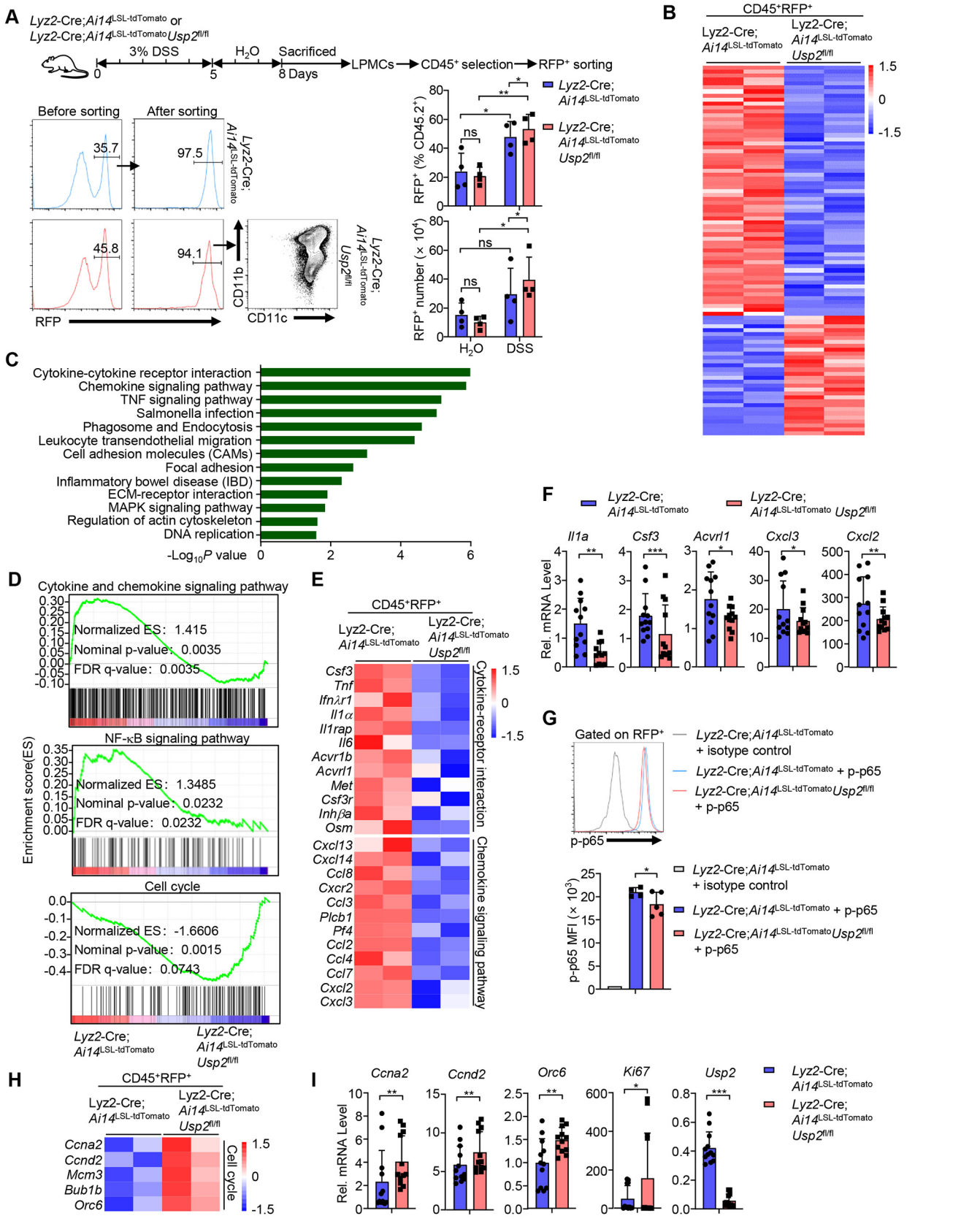

(caption on next page)

Fig. 2. USP2 alters gene expression profile in myeloid cells after DSS treatment.
(A) Schematic illustration of acquisition of colonic RFP$^+$ cells from *Lyz2*-Cre;*Ai14*$^{LSL\text{-}tdTomato}$ or *Lyz2*-Cre;*Ai14*$^{LSL\text{-}tdTomato}$*Usp2*$^{fl/fl}$ mice, flow cytometry analysis of purities of RFP$^+$ cells in LPMCs from *Lyz2*-Cre;*Ai14*$^{LSL\text{-}tdTomato}$ and *Lyz2*-Cre;*Ai14*$^{LSL\text{-}tdTomato}$*Usp2*$^{fl/fl}$ mice before and after flow sorting, and components of RFP$^+$ cells in LPMCs from *Lyz2*-Cre;*Ai14*$^{LSL\text{-}tdTomato}$ and *Lyz2*-Cre;*Ai14*$^{LSL\text{-}tdTomato}$*Usp2*$^{fl/fl}$ mice after DSS treatment, and proportions and numbers of RFP$^+$ cells in LPMCs from *Lyz2*-Cre;*Ai14*$^{LSL\text{-}tdTomato}$ (n = 4) and *Lyz2*-Cre;*Ai14*$^{LSL\text{-}tdTomato}$*Usp2*$^{fl/fl}$ (n = 4) mice before and after DSS treatment.
(B) Heatmap of differentially expressed genes (DEGs) that meet the conditions of *P*-Value < 0.05 and $|\log_2$Fold change$|\geq 1$ in the transcriptome analysis of colonic RFP$^+$ cells from two groups of *Lyz2*-Cre;*Ai14*$^{LSL\text{-}tdTomato}$ (n = 11) and *Lyz2*-Cre;*Ai14*$^{LSL\text{-}tdTomato}$*Usp2*$^{fl/fl}$ mice (n = 9) with DSS-induced colitis.
(C) KEGG pathway enriched by DEGs in the transcriptome analysis of colonic RFP$^+$ cells from two groups of *Lyz2*-Cre;*Ai14*$^{LSL\text{-}tdTomato}$ (n = 11) and *Lyz2*-Cre;*Ai14*$^{LSL\text{-}tdTomato}$*Usp2*$^{fl/fl}$ (n = 9) mice with DSS-induced colitis.
(D) GSEA analysis of cytokine and chemokine signaling pathway, NF-κB signaling pathway, and cell cycle signaling pathway from the transcriptome data of colonic RFP$^+$ cells from two groups of *Lyz2*-Cre;*Ai14*$^{LSL\text{-}tdTomato}$ (n = 11) and *Lyz2*-Cre;*Ai14*$^{LSL\text{-}tdTomato}$*Usp2*$^{fl/fl}$ (n = 9) mice with DSS-induced colitis.
(E) Heatmap of the indicated genes related cytokine and chemokine signaling pathway from the transcriptome data of colonic RFP$^+$ cells from two groups of *Lyz2*-Cre;*Ai14*$^{LSL\text{-}tdTomato}$ (n = 11) and *Lyz2*-Cre;*Ai14*$^{LSL\text{-}tdTomato}$*Usp2*$^{fl/fl}$ (n = 9) mice with DSS-induced colitis.
(F) qRT-PCR results of the signature genes for cytokines, chemokines in colonic RFP$^+$ cells from *Lyz2*-Cre;*Ai14*$^{LSL\text{-}tdTomato}$ (n = 12) and *Lyz2*-Cre;*Ai14*$^{LSL\text{-}tdTomato}$*Usp2*$^{fl/fl}$ (n = 12) mice with DSS-induced colitis.
(G) Flow cytometry analysis and mean fluorescence intensities (MFIs) of p-p65 in RFP$^+$ cells of LPMCs from *Lyz2*-Cre;*Ai14*$^{LSL\text{-}tdTomato}$ (n = 4) and *Lyz2*-Cre;*Ai14*$^{LSL\text{-}tdTomato}$*Usp2*$^{fl/fl}$ (n = 4) mice with DSS-induced colitis.
(H) Heatmap of the indicated genes related cell cycle from the transcriptome data of colonic RFP$^+$ cells from two groups of *Lyz2*-Cre;*Ai14*$^{LSL\text{-}tdTomato}$ (n = 11) and *Lyz2*-Cre;*Ai14*$^{LSL\text{-}tdTomato}$*Usp2*$^{fl/fl}$ (n = 9) mice with DSS-induced colitis.
(I) qRT-PCR results of the signature genes for cell cycle in colonic RFP$^+$ cells from *Lyz2*-Cre;*Ai14*$^{LSL\text{-}tdTomato}$ (n = 12) and *Lyz2*-Cre;*Ai14*$^{LSL\text{-}tdTomato}$*Usp2*$^{fl/fl}$ (n = 12) mice with DSS-induced colitis.
$^*P < 0.05$, $^{**}P < 0.01$, $^{***}P < 0.001$ (Student's unpaired *t*-test for A, G or Student's paired *t*-test for F, I). ns, not significant. Graphs show mean ± S.D. (A, F, I, G). Data are representative of three (G) or a combination of three (F, I) or four (A) independent experiments.

cytokines and chemokines (*Tnf*, *Csf3*, *Cxcl3*, *Cxcl2* and *Acvrl1*) were significantly downregulated (Fig. 2E and F). Consistently, we found that the phosphorylation of p65 in *Usp2* deficient RFP$^+$ cells was significantly reduced compared with that in *Usp2* sufficient RFP$^+$ cells in DSS-induced colitis mice as revealed by flow cytometry analysis (Fig. 2G). In contrast, the genes encoding promoters for cell cycle (*Ccna2*, *Ccnd2*, *Orc6* and *Ki67*) were significantly upregulated in the *Lyz2*-Cre;*Usp2*$^{fl/fl}$*Ai14*$^{LSL-Td\text{-}Tomato}$ RFP$^+$ LPMCs compared to the *Lyz2*-Cre;*Ai14*$^{LSL-TdTomato}$ counterparts from mice induced DSS colitis (Fig. 2H and I). These data together suggest that knockout of USP2 in myeloid cells inhibits the NF-κB signaling pathway and the expression of pro-inflammatory cytokines and chemokines and promotes the expression of cell cycle-related genes in the myeloid cells of lamina propria from mice treated with DSS.

2.4. USP2 inhibits the proliferation of macrophages and dendritic cells in the lamina propria during DSS-induced colitis

We have observed comparable RFP$^+$ cells in LPMCs from the *Lyz2*-Cre;*Ai14*$^{LSL-TdTomato}$ mice and the *Lyz2*-Cre;*Usp2*$^{fl/fl}$*Ai14*$^{LSL-TdTomato}$ mice under homeostatic conditions (Fig. 2A). Consistently, we found that the percentages and the numbers of CD11c$^+$ and CD11b$^+$CD11c$^-$ cells in the lamina propria of *Lyz2*-Cre;*Usp2*$^{fl/fl}$ mice were similar to those in the lamina propria of *Usp2*$^{fl/fl}$ mice (Figs. S4A and S4B). The CD11b$^+$CD11c$^-$ population mainly consists of CD11b$^+$CD11c$^-$F4/80$^+$ macrophages and CD11b$^+$CD11c$^-$Gr-1$^+$ neutrophils (Bassler et al., 2019). We found that most of the CD11b$^+$ cells were the CD11b$^+$CD11c$^-$F4/80$^+$ macrophages and few were CD11b$^+$CD11c$^-$Gr-1$^+$ neutrophils in the lamina propria and both populations in the *Usp2*$^{fl/fl}$ mice were comparable to those of the *Lyz2*-Cre;*Usp2*$^{fl/fl}$ mice (Figs. S4A and S4C). The lamina propria CD11c$^+$ cells consist of three major subsets: CD103$^+$CD11b$^-$, CD11b$^+$CD103$^-$, and CD103$^+$CD11b$^+$ (Mencarelli et al., 2018). Similarly, the percentages and numbers of the three subsets of CD11c$^+$ cells were comparable in the lamina propria of *Usp2*$^{fl/fl}$ mice and *Lyz2*-Cre;*Usp2*$^{fl/fl}$ mice (Figs. S4A and S4D). In addition, the percentages and numbers of IFNγ-producing CD4$^+$ T cells or CD8$^+$ T cells, IL-17A- or FoxP3-expressing CD4$^+$ T cells were not affected in the lamina propria of *Lyz2*-Cre;*Usp2*$^{fl/fl}$ mice compared to *Usp2*$^{fl/fl}$ mice (Figs. S4E and S4F), indicating that USP2 is dispensable for the homeostasis of immune cells in the lamina propria of mice without DSS treatment.

We next examined the compositions of myeloid cells in the colonic lamina propria of *Usp2*$^{fl/fl}$ and *Lyz2*-Cre;*Usp2*$^{fl/fl}$ mice during DSS-induced colitis. Results from flow cytometry assays suggested that the percentages and the numbers of CD11c$^+$ and CD11b$^+$CD11c$^-$ cells were significantly increased in the lamina propria of *Lyz2*-Cre;*Usp2*$^{fl/fl}$ mice compared to *Usp2*$^{fl/fl}$ mice (Fig. 3A and B). Interestingly, the percentages of CD11b$^+$CD11c$^-$F4/80$^+$ macrophages were higher and the percentages of CD11b$^+$CD11c$^-$Gr-1$^+$ neutrophils were lower in the lamina propria of *Lyz2*-Cre;*Usp2*$^{fl/fl}$ mice than in the lamina propria of *Usp2*$^{fl/fl}$ mice, respectively (Fig. 3A and C). Consequently, the numbers of CD11b$^+$CD11c$^-$F4/80$^+$ macrophages but not CD11b$^+$CD11c$^-$Gr-1$^+$ neutrophils were significantly more in the lamina propria of *Lyz2*-Cre;*Usp2*$^{fl/fl}$ mice than in the lamina propria of *Usp2*$^{fl/fl}$ mice (Fig. 3C). We found that the percentages of CD103$^+$, CD11b$^+$ and CD103$^+$CD11b$^+$ dendritic cells were similar in the lamina propria CD11c$^+$ population of *Lyz2*-Cre;*Usp2*$^{fl/fl}$ mice to those of *Usp2*$^{fl/fl}$ mice (Fig. 3A and D). However, the numbers of CD103$^+$ and CD11b$^+$ dendritic cells were significantly more in the lamina propria of *Lyz2*-Cre;*Usp2*$^{fl/fl}$ mice than *Usp2*$^{fl/fl}$ mice (Fig. 3D). The analyses of transcriptomic data have suggested the upregulation of cell cycle pathways in USP2-dificient myeloid cells versus USP2-sufficient counterparts after induction of colitis (Fig. 2D). Consistent with the observations, we found that the percentages of Ki67 staining in CD11b$^+$CD11c$^-$F4/80$^+$ macrophages, CD11c$^+$CD103$^+$ and CD11c$^+$CD11b$^+$ dendritic cells were significantly higher in the lamina propria of *Lyz2*-Cre;*Usp2*$^{fl/fl}$ mice than in the lamina propria of *Usp2*$^{fl/fl}$ mice (Fig. 3E), indicating a cytostatic role of USP2 in myeloid cells.

We have previously reported USP2 tunes up TGF-β signaling to promote the expression of cell cycle inhibitory genes in various tumor cell lines such as HeLa, Hep3B, HCT116 and 4T1 and primary lung epithelial cells by deubiquitinating TGFBR1 (Zhao et al., 2018). In this context, we examined whether USP2 regulates proliferation of myeloid cells by TGF-β signaling. Interestingly, however, results from flow cytometry analysis showed that the level of p-SMAD2 was significantly upregulated in the *Lyz2*-Cre;*Usp2*$^{fl/fl}$*Ai14*$^{LSL-TdTomato}$ RFP$^+$ LPMCs compared to the *Lyz2*-Cre;*Ai14*$^{LSL-TdTomato}$ counterparts from mice induced DSS colitis (Fig. S5A), indicating an inhibitory role of USP2 in TGF-β signaling in myeloid cells under inflammatory conditions. To examine whether USP2 directly regulates TGF-β signaling in vitro, we isolated RFP$^+$ LPMCs from *Lyz2*-Cre;*Usp2*$^{fl/fl}$*Ai14*$^{LSL-TdTomato}$ and *Lyz2*-Cre;*Ai14*$^{LSL-TdTomato}$ mice and stimulated them with TGF-β for 30 min or 4 h followed by flow cytometry with p-SMAD2 and Ki67. Consistently, we found that the levels of p-SMAD2 and Ki67 were significantly upregulated in RFP$^+$ LPMCs from *Lyz2*-Cre;*Usp2*$^{fl/fl}$*Ai14*$^{LSL-TdTomato}$ mice compared to those from *Lyz2*-Cre;*Ai14*$^{LSL-TdTomato}$ mice (Figs. S5B and S5C), suggesting that USP2 down-regulates TGF-β pathway to inhibit proliferation of RFP$^+$ cells. These results together suggest that USP2 suppresses the proliferation of CD11b$^+$CD11c$^-$F4/80$^+$ macrophages, CD11c$^+$CD103$^+$

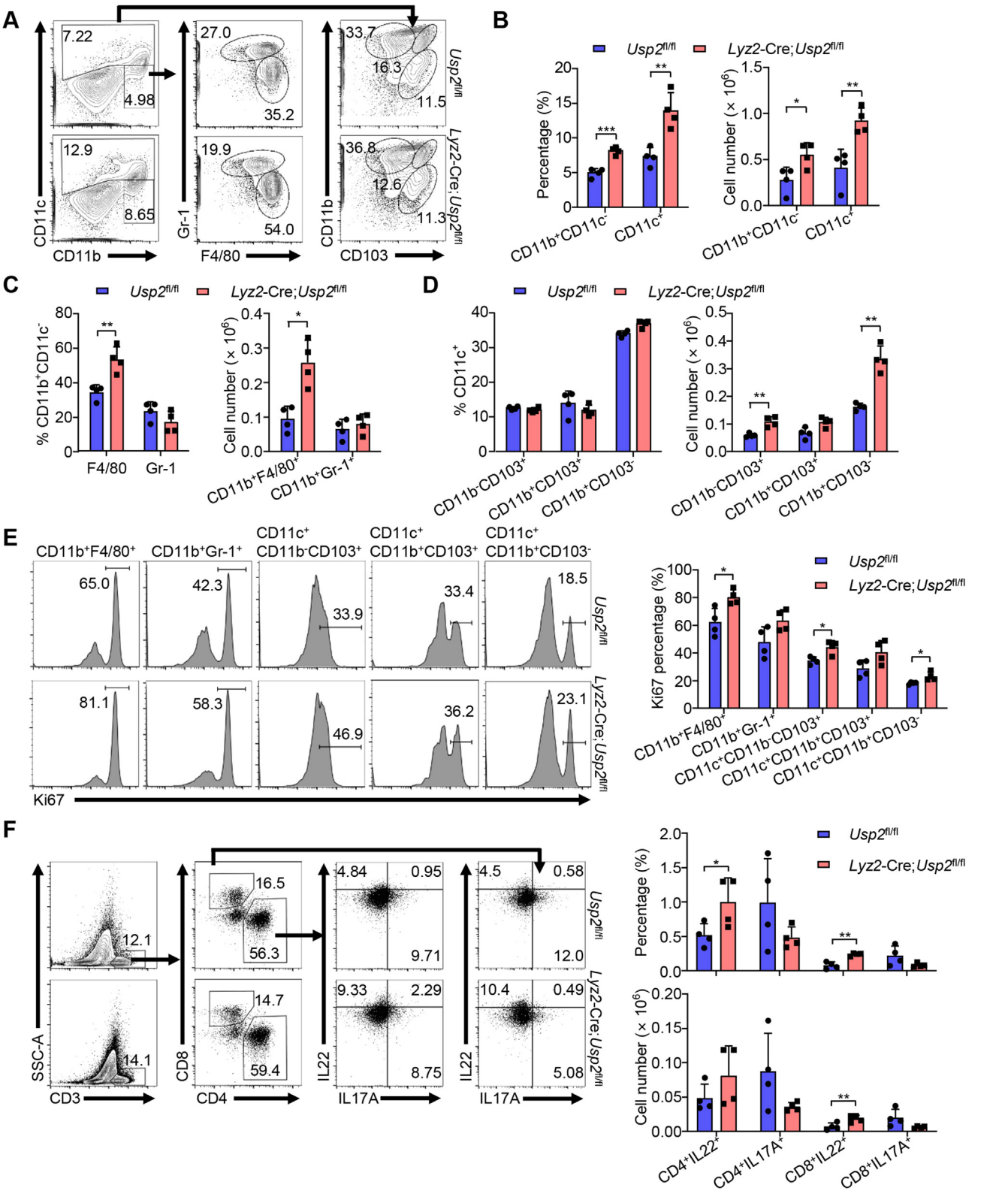

(caption on next page)

Fig. 3. USP2 inhibits the proliferation of macrophages and dendritic cells to promote type I immune responses in the lamina propria during DSS-induced colitis.

(A) Flow cytometry analysis of myeloid cells in LPMCs from *Usp2*$^{fl/fl}$ (n = 4) and *Lyz2*-Cre;*Usp2*$^{fl/fl}$ (n = 4) mice with DSS-induced colitis.

(B) The proportions and numbers of CD11b^{+}CD11c^{-} and CD11c^{+} cells in LPMCs from *Usp2*$^{fl/fl}$ (n = 4) and *Lyz2*-Cre;*Usp2*$^{fl/fl}$ (n = 4) mice with DSS-induced colitis.

(C) The proportions and numbers of CD11b^{+}F4/80^{+} macrophages and CD11b^{+}Gr-1^{+} neutrophils in LPMCs from *Usp2*$^{fl/fl}$ (n = 4) and *Lyz2*-Cre;*Usp2*$^{fl/fl}$ (n = 4) mice with DSS-induced colitis.

(D) The proportions and numbers of CD11b^{-}CD103^{+}, CD11b^{+}CD103^{+}, CD11b^{+}CD103^{-} DCs in LPMCs from *Usp2*$^{fl/fl}$ (n = 4) and *Lyz2*-Cre;*Usp2*$^{fl/fl}$ (n = 4) mice with DSS-induced colitis.

(E) Flow cytometry analysis of proportions of Ki67 in CD11b^{+}F4/80^{+} macrophages, CD11b^{+}Gr-1^{+} neutrophils, CD11c^{+}CD11b^{-}CD103^{+}, CD11c^{+}CD11b^{+}CD103^{+} and CD11c^{+}CD11b^{+}CD103^{-} DCs of LPMCs from *Usp2*$^{fl/fl}$ (n = 4) and *Lyz2*-Cre;*Usp2*$^{fl/fl}$ (n = 4) mice with DSS-induced colitis.

(F) Flow cytometry analysis and the proportions and numbers of IL-22-and IL-17A-producing T lymphocytes in LPMCs from *Usp2*$^{fl/fl}$ (n = 4) and *Lyz2*-Cre;*Usp2*$^{fl/fl}$ (n = 4) mice with DSS-induced colitis.

$^{*}P < 0.05$, $^{**}P < 0.01$, $^{***}P < 0.001$ (Student's unpaired *t*-test). Graphs show mean ± S.D. (B–F). Data are representative of two (A–F).

and CD11c^{+}CD11b^{+} dendritic cells in the lamina propria during DSS-induced colitis by inhibiting the activation of TGF-β signaling pathway.

2.5. Knockout of USP2 in myeloid cells promotes the generation of IL-22- and IFNγ-producing T cells in the lamina propria

A major function of the macrophages and dendritic cells in the lamina propria is to present antigens to and activate T cells (Thery and Amigorena, 2001). We found that the percentages and the numbers of IL-22- or IFNγ-producing but not IL-17A-producing CD4^{+} T cells and CD8^{+} T cells were significantly increased in the lamina propria from *Lyz2*-Cre;*Usp2*$^{fl/fl}$ mice compared to those from *Usp2*$^{fl/fl}$ mice, indicating that knockout of USP2 in myeloid cells may contribute to tissue repair and promote type I immune responses in colon inflammation (Fig. 3F and Fig. S5D). In contrast, the percentages and numbers of γδ TCR^{+}IFNγ^{+}, γδ TCR^{+}IL-22^{+}, and γδ TCR^{+}IL-17A^{+} were similar in the LPMCs of colons from *Lyz2*-Cre;*Usp2*$^{fl/fl}$ and *Usp2*$^{fl/fl}$ mice (Fig. S5E), suggesting that myeloid USP2 is not involved in the activation and differentiation of γδ T cells during DSS-induced colitis. Interestingly, the surface levels of the antigen-presenting molecules including MHC-II, CD80 and CD86 were comparable between the macrophages and the dendritic cells from the lamina propria of *Lyz2*-Cre;*Usp2*$^{fl/fl}$ mice and the counterparts of *Usp2*$^{fl/fl}$ mice (Figs. S6A and S6B), indicating that USP2 does not affect the expression of antigen-presenting molecules. Taken together, these data suggest that USP2 restricts the proliferation of myeloid cells and thereby inhibits the activation and expansion of IL-22- and IFNγ-producing T cells in the lamina propria during DSS-induced colitis.

2.6. USP2 in myeloid cells inhibits immune responses to bacterial infections in the gut

The commensal bacterial infections in the gut induce severe inflammation after DSS treatment that causes epithelium damage, while the immune cells in the lamina propria restricts the infections and thereby alleviates inflammation (Strober et al., 2007). Because myeloid USP2 negatively regulates type I immune responses, we next investigated whether USP2 regulated antibacterial immune responses in the gut. The *Lyz2*-Cre;*Usp2*$^{fl/fl}$ mice and the *Usp2*$^{fl/fl}$ mice were infected with *Citrobacter rodentium* by gavage and the body weight and fecal bacteria count were monitored (Fig. 4A). The results suggested that *Lyz2*-Cre;*Usp2*$^{fl/fl}$ mice had more constant gain of weight than *Usp2*$^{fl/fl}$ mice and the fecal bacteria counts of *Lyz2*-Cre;*Usp2*$^{fl/fl}$ mice were significantly lower than that of *Usp2*$^{fl/fl}$ mice (Fig. 4A and B). In addition, the percentages of CD11c^{+} population, CD11c^{+}CD103^{+} and CD11c^{+}CD11b^{+} dendritic cells were significantly increased, whereas the percentages of CD11b^{+}CD11c^{-} population and CD11b^{+}F4/80^{+} macrophage were similar in the lamina propria of *Lyz2*-Cre;*Usp2*$^{fl/fl}$ mice to those of *Usp2*$^{fl/fl}$ mice (Fig. 4C). Consistently, the expression levels of Ki67 in CD11c^{+}, CD11c^{+}CD103^{+} and CD11c^{+}CD11b^{+} cells of lamina propria were higher in *Lyz2*-Cre;*Usp2*$^{fl/fl}$ mice than those in *Usp2*$^{fl/fl}$ mice (Fig. 4D). Furthermore, the IFNγ-producing CD4^{+} T and CD8^{+} T cells in the lamina propria were significantly more and the *Ifng* mRNA levels in the colon tissues were higher in the *Lyz2*-Cre;*Usp2*$^{fl/fl}$ mice than the *Usp2*$^{fl/fl}$ mice (Fig. 4E and F). Collectively, these data suggest that knockout of USP2 inhibits expansion of dendritic cells to turn down T cell activation, and thereby aggravates bacterial infections in the gut.

2.7. Knockout of USP2 in myeloid cells alters the extracellular matrix in the inflamed colon

In addition to presenting antigen for T cell activation, the myeloid cells communicate with the epithelium for tissue repair through remodeling the extracellular matrix (ECM) during inflammation (Quiros and Nusrat, 2019). Specifically, the cytokines and chemokines originating from myeloid cells induce the expression of ECM-related genes in the epithelium (Lawrance et al., 2017; Wang et al., 2021). In support of this notion, KEGG and GSEA analyses of the transcriptomic data revealed that the cytokines and chemokines pathway, ECM-receptor interaction pathway and fibrogenic pathway genes (Lawrance et al., 2017; Wang et al., 2021) were significantly downregulated in *Lyz2*-Cre;*Usp2*$^{fl/fl}$*Ai14*$^{LSL-TdTomato}$ colonic RFP^{+} cells compared to the *Lyz2*-Cre;*Ai14*$^{LSL-TdTomato}$ counterparts, which was confirmed by qRT-PCR analyses (Fig. 5A and B). Consistently, the mRNA levels of ECM-related genes including *Col4a1*, *Col4a2*, *Col1a1*, *Sdc4*, *Thbs1* and *Lamb1* were significantly downregulated in the inflamed colon tissues of *Lyz2*-Cre;*Usp2*$^{fl/fl}$ mice than *Usp2*$^{fl/fl}$ mice (Fig. 5C). In addition, results from Masson trichromatic staining showed that collagens (major components of ECM in the gut) (Rieder et al., 2013) accumulated more intensively in the colon tissues from *Usp2*$^{fl/fl}$ mice than *Lyz2*-Cre;*Usp2*$^{fl/fl}$ mice after colitis induction (Fig. 5D), indicating that knockout of USP2 impairs the ECM remodeling in the colon inflammation. Dysregulated ECM would promote inflammation and inflammation-related fibrosis that is characterized by α-SMA (Rathinam and Chan, 2018). Results from qRT-PCR and immunohistochemistry (IHC) assays suggested that the mRNA and protein levels of α-SMA were significantly lower in colon tissues of *Lyz2*-Cre;*Usp2*$^{fl/fl}$ mice than *Usp2*$^{fl/fl}$ mice after colitis induction (Fig. 5C and D). These data together suggest that knockout of USP2 in myeloid cells inhibits dysregulation of ECM in the colon after DSS treatment.

To further confirm that the myeloid cells trained the epithelium to induce dysregulation of ECM, we isolated RFP^{+} cells from the LPMCs of *Lyz2*-Cre;*Usp2*$^{fl/fl}$*Ai14*$^{LSL-TdTomato}$ mice *Lyz2*-Cre;*Ai14*$^{LSL-TdTomato}$ mice that were treated with DSS and cultured these cells for 18 h. The conditioned medium (CM) of cultured RFP^{+} cells were used to stimulate colon organoids for 24 h followed by qRT-PCR assays (Fig. 5E). The results suggested that the CM of *Lyz2*-Cre;*Ai14*$^{LSL-TdTomato}$ RFP^{+} cells induced upregulation of ECM-related genes such as *Col4a1*, *Thbs1* and *Acta2* more profoundly than did the CM of *Lyz2*-Cre;*Usp2*$^{fl/fl}$*Ai14*$^{LSL-TdTomato}$ RFP^{+} cells (Fig. 5F). These data indicate that USP2-mediated myeloid-derived signals induce upregulation of ECM during inflammation in the gut.

We found that knockout of USP2 in myeloid cells promoted the generation of IL-22-producing T cells (Fig. 3F) and the expansion of CD11b^{+}F4/80^{+} macrophages, which play essential roles in gut epithelial

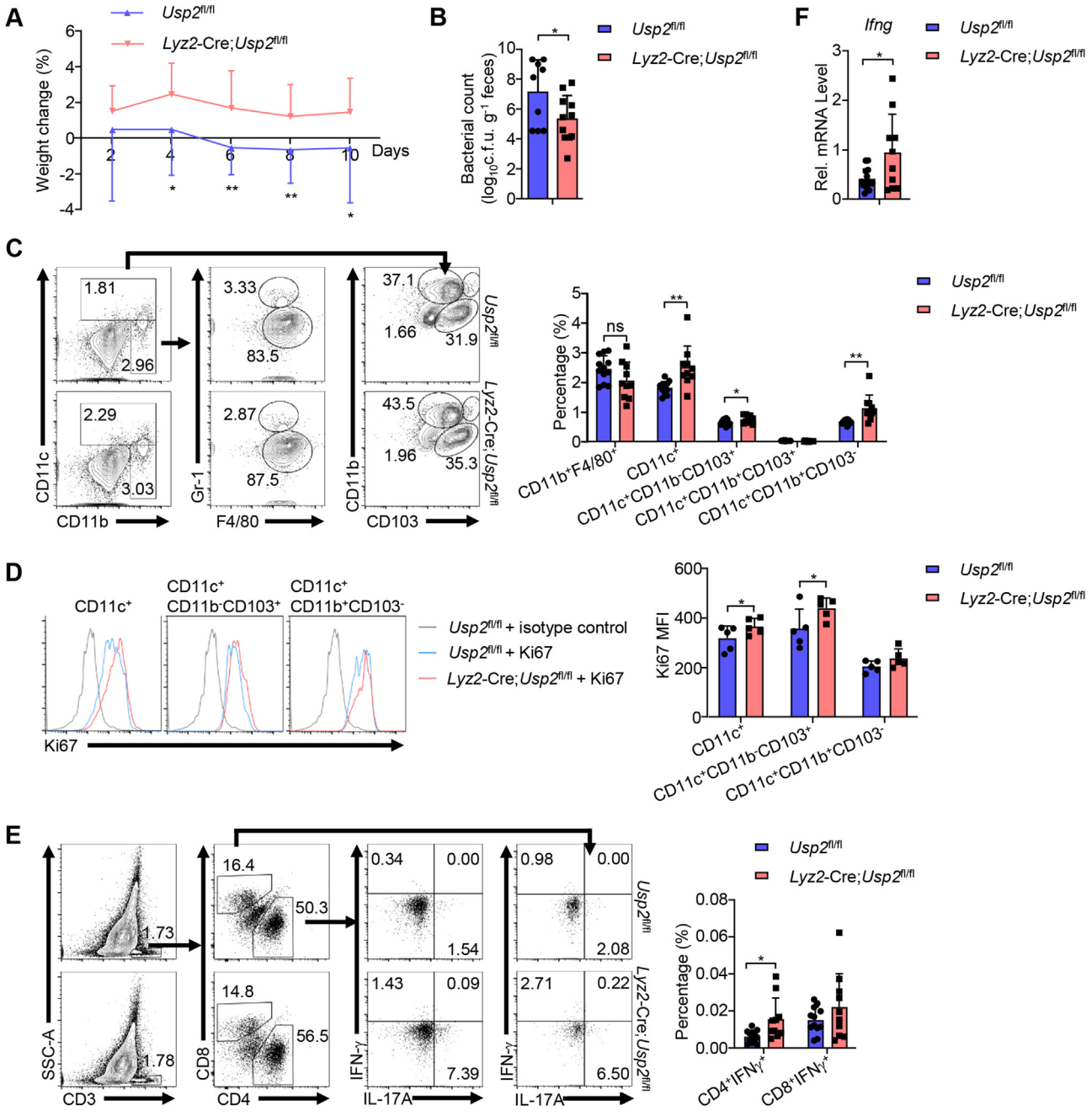

Fig. 4. USP2 in myeloid cells inhibits immune responses to bacterial infections in the gut.

(A) Body weight change of *Usp2*$^{fl/fl}$ (n = 16) and *Lyz2*-Cre;*Usp2*$^{fl/fl}$ (n = 14) mice that were injected with 1 × 10^9 colony-forming units (c.f.u.) of *Citrobacter rodentium* by gavage.

(B) Bacterial counts of *Usp2*$^{fl/fl}$ (n = 9) and *Lyz2*-Cre;*Usp2*$^{fl/fl}$ (n = 11) mice at day 6 after injection of *Citrobacter rodentium* (1 × 10^9 c.f.u.) by gavage.

(C) Flow cytometry analysis and proportions of CD11b$^+$F4/80$^+$ macrophages, CD11c$^+$CD11b$^-$CD103$^+$, CD11c$^+$CD11b$^+$CD103$^+$ and CD11c$^+$CD11b$^+$CD103$^-$ DCs in LPMCs from *Usp2*$^{fl/fl}$ (n = 12) and *Lyz2*-Cre;*Usp2*$^{fl/fl}$ (n = 10) mice that were treated as in (A).

(D) Flow cytometry analysis and mean fluorescence intensities (MFIs) of Ki67 in CD11c$^+$, CD11c$^+$CD11b$^-$CD103$^+$ and CD11c$^+$CD11b$^+$CD103$^-$ DCs of LPMCs from *Usp2*$^{fl/fl}$ (n = 5) and *Lyz2*-Cre;*Usp2*$^{fl/fl}$ (n = 5) mice that were treated as in (A).

(E) Flow cytometry analysis and proportions of IFNγ-producing T lymphocytes in LPMCs from *Usp2*$^{fl/fl}$ (n = 12) and *Lyz2*-Cre;*Usp2*$^{fl/fl}$ (n = 10) mice that were treated as in (A).

(F) qRT-PCR results of *Ifng* in colon tissues from *Usp2*$^{fl/fl}$ (n = 14) and *Lyz2*-Cre;*Usp2*$^{fl/fl}$ (n = 10) mice that were treated as in (A).

*P < 0.05, **P < 0.01, ***P < 0.001 (Student's unpaired t-test). ns, not significant. Graphs show mean ± S.D. (A–F). Data are a combination of two (A-C, E-F) independent experiments or representative of two (D) independent experiments.

repair (Quiros and Nusrat, 2019; Sugimoto et al., 2008). We next examined whether knockout of USP2 in myeloid cells promoted tissue repair during DSS-induced colitis. Firstly, we examined the expression of tight junction proteins such as ZO-1 and Occludin in intestinal epithelium of mice with DSS-induced colitis (Gunzel and Yu, 2013), and found that the expression levels of ZO-1 and Occludin were higher in the epithelium of inflammatory colon tissues of *Lyz2*-Cre;*Usp2*$^{fl/fl}$ mice than those of *Usp2*$^{fl/fl}$ mice (Fig. 5G). Secondly, we examined the intestinal permeability by gavage of Fluorescein isothiocyanate-dextran (FD-40) in DSS-treated mice followed by detection of FD-40 in sera (Oami and Coopersmith, 2021). The results suggested that the level of FD-40 was significantly lower in the sera from *Lyz2*-Cre;*Usp2*$^{fl/fl}$ mice compared to *Usp2*$^{fl/fl}$ mice (Fig. 5H). Collectively, these results indicate that USP2 in myeloid cells destroys the integrity of intestinal barrier during DSS-induced colitis.

2.8. Pharmacological inhibition of USP2 inhibits DSS-induced colitis

Because USP2 is a deubiquitinating enzyme and ML364 is a specific inhibitor for USP2, we next examined whether targeting USP2 by ML364 inhibited DSS-induced colitis. The wild-type C57BL/6 were fed with 3% DSS for 5 d followed by normal sterile water for 3 d. On day 0, the mice were intraperitoneally injected with ML364 (10 mg/kg bodyweight) or DMSO once a day for 8 d (Fig. 6A). The results suggested that mice treated with ML364 exhibited less weight loss, longer colon and milder ulcers in the colon than mice treated with DMSO (Fig. 6B and C), suggesting that inhibition of USP2 protects mice from DSS-induced colitis. In addition, the percentages of CD11b$^+$F4/80$^+$ macrophages and CD11c$^+$CD103$^+$ and CD11c$^+$CD11b$^+$ dendritic cells in the lamina propria and the percentages of Ki67 staining in those cells were significantly increased in mice treated with ML364 compared to those in mice treated with DMSO (Fig. 6D and E), indicating that inhibition of USP2 leads to hyper-proliferation of macrophages and dendritic cells in the gut during inflammation. Consistently, the generation of IL-22-producing T cells and type I immune responses were potentiated in the gut of mice treated with ML364 compared to DMSO, as monitored by the increased IL-22- and IFNγ-producing CD4$^+$ T and CD8$^+$ T cells in the LPMCs in mice treated with ML364 (Fig. 6F). These data together suggest that inhibition of USP2 promotes the proliferation of macrophages and dendritic cells to activate IL-22- and IFNγ-producing T cells during DSS-induced colitis.

We also examined whether targeting USP2 by ML364 inhibited the dysregulation of ECM and promoted tissue repair. As shown in Fig. 7A, the accumulation of collagens was substantially impaired in the colon tissues from mice treated with ML364 compared to that from mice treated with DMSO. Consistent with the observation, the levels of ECM-related genes and α-SMA were substantially inhibited in the colon tissues of mice treated with ML364 compared to those of mice treated with DMSO (Fig. 7A and B). Moreover, the expression levels of ZO-1, Occludin were higher in the colon tissues from mice treated with ML364 compared to those from mice treated with DMSO (Fig. 7C). The levels of FD-40 in the sera of mice treated with ML364 were significantly lower than those from mice treated with DMSO (Fig. 7D), indicating that inhibition of USP2 promotes the gut epithelial integrity after DSS treatment. Taken together, these data suggest that pharmacological inhibition of USP2 prevents dysregulation of ECM and promotes the integrity of the epithelial barrier in the gut during inflammation, and that targeting USP2 might provide a potential strategy for therapeutic intervention of inflammatory diseases in the gut.

3. Discussion

IBD is a chronic, relapsing-remitting inflammatory gastrointestinal disease usually with unknown etiology and the number of affecting patients has been increasing for decades. Identification of potential factors and characterization of their roles and mechanisms in IBD would provide insight into the treatment of IBD. Here in this study, we have provided evidence that USP2 promotes experimental colitis and that targeting USP2 by small molecules inhibited DSS-induced colitis in mice, suggesting USP2 as a potential target for treatment of IBD (Fig. 7E). By analyzing the transcriptomic data from the colonic biopsies of UC patients, we have found that USP2 was highly expressed in the inflamed mucosa compared to the normal adjacent mucosal tissues. In addition, the expression of USP2 was significantly increased in the colonic LPMCs from mice treated with DSS, a mouse colitis model resembling human IBD. Interestingly, we found that *Lyz2*-Cre- but not CD4-Cre- or *Vil*-Cre-mediated deletion of USP2 alleviated DSS-induced colitis, indicating an essential role of USP2 in myeloid cells in promoting gastrointestinal inflammation. Results from gene expression profiling assays suggested that knockout of USP2 resulted in upregulation of cell cycle and DNA replication pathways in lamina propria myeloid cells after DSS treatment. Consistent with these observations, we observed that the numbers and percentages of CD11b$^+$ macrophages and CD11c$^+$CD11b$^+$ and CD11c$^+$CD11b$^+$ dendritic cells were significantly increased in the lamina propria from *Lyz2*-Cre;*Usp2*$^{fl/fl}$ mice compared to *Usp2*$^{fl/fl}$ mice. These findings suggest an inhibitory role of USP2 in the proliferation of myeloid cells in the context of colon inflammation.

It has been shown that USP2 promotes cell proliferation of bladder (Kim et al., 2012), prostate (Stevenson et al., 2007), pancreatic (Shi et al., 2011), and inhibits clear renal carcinoma cell lines proliferation (Meng et al., 2020). However, we found that USP2 inhibited the cell cycle and the proliferation of lamina propria macrophages and dendritic cells during DSS-induced colitis. These different regulatory roles of USP2 in cell cycle are possibly due to distinct targets of USP2 in distinct cell types. We have previously reported that USP2 positively regulates TGF-β signaling in tumor parenchymal cells by promoting deubiquitylation of TGFBR1 and participates in tumor genesis and metastasis (Zhao et al., 2018). In contrast, we found that USP2 inhibits the TGF-β signaling and the proliferation of myeloid cells. In support of this notion, a number of studies have shown that TGFβ signaling promotes the proliferation of myeloid cells (Bataller et al., 2019; Huang et al., 2020; Meng et al., 2016). Moreover, a recent study has reported that USP2 inhibits TGF-β pathway by promoting deubiquitylation of SMAD7 in glioblastoma cells that has been assumed to originate from glial-type cells and resembles some features of glial macrophages (Tu et al., 2022). Whether USP2 down-regulates TGF-β pathway dependently on SMAD7 in myeloid cells in such a context as DSS treatment requires further investigation. Collectively, these data suggest that USP2 negatively regulates TGF-β signaling to suppress myeloid cells proliferation in the lamina propria during DSS-induced colitis, although it promotes TGF-β signaling and exhibits cytostatic effects in multiple non-immune cells.

One major function of myeloid cells is to activate T cells during infection and inflammation. Although the expression of antigen presenting-related molecules was comparable in macrophages or dendritic cells from the *Lyz2*-Cre;*Usp2*$^{fl/fl}$ and *Usp2*$^{fl/fl}$ mice, the percentages and numbers of IL-22- and IFNγ-producing CD4$^+$ T cells and CD8$^+$ T cells in the lamina propria from *Lyz2*-Cre;*Usp2*$^{fl/fl}$ mice were significantly increased compared to those from *Usp2*$^{fl/fl}$ mice after DSS treatment. We found that the CD11c$^+$ and CD11b$^+$ myeloid cells exhibited hyper-proliferation compared to the control cells and the numbers of CD11c$^+$ and CD11b$^+$ myeloid cells were significantly increased in the LPMCs from *Lyz2*-Cre;*Usp2*$^{fl/fl}$ mice compared to *Usp2*$^{fl/fl}$ mice after DSS induction, which might be responsible for the potentiated the generation of IL-22- and IFNγ-producing T cells. Type I immune responses are known to defend against bacterial infection (Billiau and Matthys, 2009). Consistent with this notion, USP2 deficiency in myeloid cells mainly dendritic cells exhibits hyper-immune responses to *Citrobacter rodentium* infection. These data indicate myeloid USP2 in promoting bacterial infection and inflammation through the myeloid-T cell axis.

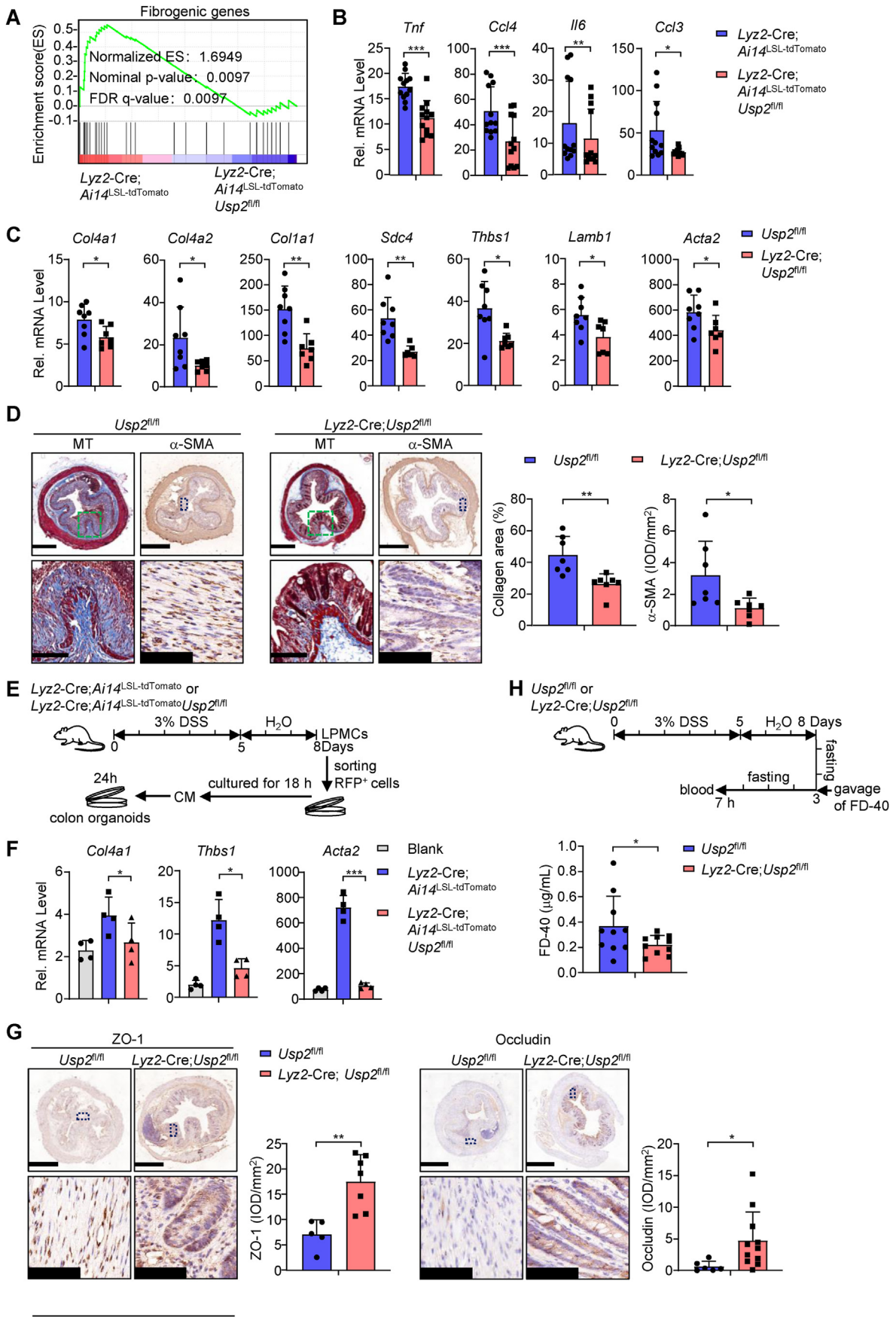

(caption on next page)

Fig. 5. Knockout of USP2 in myeloid cells alters the extracellular matrix in the inflamed colon.
(A) GSEA analysis of fibrogenic genes from the transcriptome data of colonic RFP$^+$ cells from two groups of *Lyz2*-Cre;*Ai14*$^{\text{LSL-tdTomato}}$ (n = 11) and *Lyz2*-Cre;*Ai14*$^{\text{LSL-tdTomato}}$*Usp2*$^{\text{fl/fl}}$ (n = 9) mice with DSS-induced colitis.
(B) qRT-PCR results of the signature fibrogenic genes in colonic RFP$^+$ cells from *Lyz2*-Cre;*Ai14*$^{\text{LSL-tdTomato}}$ (n = 12) and *Lyz2*-Cre;*Ai14*$^{\text{LSL-tdTomato}}$*Usp2*$^{\text{fl/fl}}$ (n = 12) mice with DSS-induced colitis.
(C) qRT-PCR results of ECM-related genes in colon tissues from *Usp2*$^{\text{fl/fl}}$ (n = 8) and *Lyz2*-Cre;*Usp2*$^{\text{fl/fl}}$ (n = 7) mice with DSS-induced colitis.
(D) Masson staining and anti-α-SMA immunohistochemistry staining, the percentage of collagen-positive areas and the integral optical density (IOD) per mm^2 analysis of α-SMA in colon sections of *Usp2*$^{\text{fl/fl}}$ (n = 7) and *Lyz2*-Cre;*Usp2*$^{\text{fl/fl}}$ (n = 7) mice with DSS-induced colitis.
(E) Schematic illustration of culturing WT colon organoids with conditioned medium.
(F) qRT-PCR results of ECM-related genes in WT colon organoids cultured with conditioned medium.
(G) Anti-ZO-1 and anti-Occludin immunohistochemistry staining, the integral optical density (IOD) per mm^2 analysis of ZO-1 and Occludin in colon sections of *Usp2*$^{\text{fl/fl}}$ (n = 5; 6) and *Lyz2*-Cre;*Usp2*$^{\text{fl/fl}}$ (n = 7; 11) mice with DSS-induced colitis.
(H) Schematic illustration and the concentration of FD-40 in peripheral blood of posterior orbital venous plexus from *Usp2*$^{\text{fl/fl}}$ (n = 10) and *Lyz2*-Cre;*Usp2*$^{\text{fl/fl}}$ (n = 10) mice with DSS-induced colitis.
$^*P < 0.05$, $^{**}P < 0.01$, $^{***}P < 0.001$ (Student's paired *t*-test for B or Student's unpaired *t*-test for C-D, F–H). Scale bars represent 600 μm, 200 μm and 100 μm. Graphs show mean ± S.D. (B-D, F–H). Data are a combination of three (B) or two (C-D, G-H) independent experiments or representative of two (F) independent experiments.

Results from our transcriptomic data suggested downregulation of cytokine and chemokine pathways in USP2 knockout myeloid cells in the lamina propria after DSS treatment, which might be responsible for the impairment of DSS-induced colitis. In this context, depletion of proinflammatory cytokines, such as IL-1β and TNF, alleviates DSS-induced colitis (Karki et al., 2017; Pugliese et al., 2017). Our results further demonstrated that USP2 promoted the phosphorylation of p65 and positively regulated the NF-κB signaling pathway in myeloid cells of inflammatory colon tissues. USP2 has been reported to directly stabilize TNF-α, contributing to LPS-mediated activation of NF-κB signaling pathway in RAW264.7 cells (Sun et al., 2016) or promote the NF-κB activation by potentiating the interaction between TRAF6 and CBM complex in T-lymphocytes (Li et al., 2013b). Whether USP2 positively regulates NF-κB activation in myeloid cells by targeting for TNF-α or TRAF6-CBM complex requires further investigations. Noteworthy, USP2 did not affect immune homeostasis of mice under homeostasis, suggesting an inflammatory environment as a prerequisite for the function of USP2. Furthermore, the potentiated type I immune responses in *Lyz2*-Cre;*Usp2*$^{\text{fl/fl}}$ mice promoted the clearance of invasive harmful bacteria, and thereby prevented sustaining inflammation in the gut, which finally leads to the downregulation of proinflammatory cytokines in USP2 deficient myeloid cells during DSS-induced colitis.

During tissue repair, epithelial cells rapidly produce a number of ECM molecules that remodel dynamically for tissue resilience and architecture (Shu and Lovicu, 2017). Such a process also requires the engagement and infiltration of growth factors, other cytokines, and chemokines produced by myeloid cells or T cells in the infections and injury sites. However, uncontrolled production of cytokines and chemokines is accompanied by chronic or severe inflammation, which finally leads to the aberrant deposition of ECM and the non-functional mass of fibrotic tissue. In this context, we found that USP2 deficiency substantially downregulates the levels of ECM-related genes, the intensities of α-SMA and promotes the generation of IL-22-producing T cells in the colon tissues after DSS treatment, suggesting an indispensable role of USP2 in the regulation of ECM and tissue repair in the gut. Moreover, one report recently showed that USP2 is involved in the angiotensin II (Ang II)-induced cardiac fibrosis via deubiquitinating and stabilizing β-catenin (Xu et al., 2021). Whether USP2 targets β-catenin for fibrogenesis in the gut deserves further investigations.

Knockout of USP2 does not affect the growth and immune cell homeostasis in the lymphatic tissues (Zhao et al., 2018), suggesting that USP2 is not involved in the homeostasis of immune cells. However, under the condition of colitis induction, targeting USP2 by ML364 promotes the proliferation of myeloid cells and the activation and expansion of IL-22- and IFNγ-producing T cells, alleviates dysregulation of ECM and protects the integrity of the colon epithelial barrier, suggesting that USP2 functions in a manner dependent on its DUB activity. Therefore, targeting the DUB activity of USP2 might provide a potential therapeutic strategy for IBD and gut infections.

4. Methods

4.1. Mice

The *Usp2*$^{+/+}$ and *Usp2*$^{-/-}$ mice were previously described (Zhao et al., 2018). *Usp2*$^{\text{fl/+}}$ mice were generated by Beijing Biocytogen Co. Ltd. Briefly speaking, guide RNAs (5′-CTTGGGAACACGGTAAGTTCCTC CC-3′, 5′-CTGCGATGTGGTAGCAAC CTCAAGA-3′ and 5′-TCCACATCT GTCGCCCCTTTTCTTC-3′) were obtained through transcription and purification in vitro. The guide RNAs were incubated with purified Cas9 protein and injected into the fertilized eggs (at the one-cell stage) together with the targeting vector with two loxp sites flanking the exons composed of exon 4, 5, and 6 of the *Usp2* gene. The injected fertilized eggs were cultured to the two-cell stage followed by transplantation into pseudopregnant mice. The targeted genomes of F0 mice were amplified by PCR and sequenced, and the chimeras were crossed with wild-type C57BL/6 mice to obtain F1 *Usp2*$^{\text{fl/+}}$ mice. Southern blot analysis was conducted with the tail DNA from F1 mice to confirm correct recombination and exclude random insertions of the targeting vector. *Lyz2*-Cre mice were purchased from the Nanjing Biomedical Research Institute of Nanjing University. WT C57BL/6 mice and *Vil*-Cre (T000142) mice were purchased from GemPharmatech. *CD4*-Cre mice were from the Jackson Laboratory and were kindly provided by Dr. X.D. Liu (Army Medical University, Chongqing, China). *Ai14*$^{\text{LSL-TdTomato}}$ mice (B6.Cg-Gt(ROSA) 26Sor$^{\text{tm14(CAG-tdTomato)Hze}}$) were from the Jackson Laboratory and were kindly provided by Dr. Y. Zhou (Wuhan University, Wuhan, China) (Li et al., 2020). *Usp2*$^{\text{fl/fl}}$ mice were crossed with *Lyz2*-Cre mice or *Ai14*$^{\text{LSL-TdTomato}}$ mice to obtain *Lyz2*-Cre *Usp2*$^{\text{fl/+}}$ and *Lyz2*-Cre *Ai14*$^{\text{LSL-TdTomato}}$*Usp2*$^{\text{fl/+}}$ mice, respectively. Age- and sex-matched *Usp2*$^{\text{fl/fl}}$ and *Lyz2*-Cre *Usp2*$^{\text{fl/fl}}$ littermates or *Lyz2*-Cre *AI14* $^{\text{fl/fl}}$ and *Lyz2*-Cre *Ai14*$^{\text{LSL-TdTomato}}$*Usp2*$^{\text{fl/fl}}$ littermates were used in all experimental studies. All mice were housed in the specific pathogen-free animal facility at Wuhan University. All animal experiments were completed in accordance with protocols approved by the Institutional Animal Care and Use Committee of Wuhan University. The mice genotypes were identified by PCR using tail DNA, and the genotyping primers were as follows: *Usp2*$^{-/-}$ forward: 5′-CTTGGGAACACGGTAAGTTCCTCCC-3′, *Usp2*$^{-/-}$ reverse: 5′-TCCACATCTGTCGCCCCTTTTCTTC-3′;*Usp2*$^{\text{fl/fl}}$ forward: 5′-AGCCTGGAGCTGT GAGAGAGTTCAT-3′, *Usp2*$^{\text{fl/fl}}$ reverse: 5′-GGTTT TGCTTTGCTGTACCTGTGCC-3’; *Lyz2*-Cre forward: 5′-CTTGGGCTGC CAGAATTTCTC-3′, *Lyz2*-Cre reverse: 5′-CCCAGAAAT GCCA-GATTACG-3’; *Ai14*$^{\text{LSL-TdTomato}}$ forward: 5′-GGCATTAAAGCAGCGTA TCC-3′, *Ai14*$^{\text{LSL-TdTomato}}$ reverse: 5′-CTGTTCCTGTACGGCATGG-3’; *Vil*-Cre forward: 5′-TTCTCCTCTAGGCTCGTCCA-3′, *Vil*-Cre reverse: 5′-CATGTCCATCAGGTTCTTGC-3’; *CD4*-Cre forward: 5′-GCATTACC GGTCGATGCAACGAGTGATGAG-3′, *CD4*-Cre reverse: 5′-GAGTGAACG AACCTGGTCGAAATCAGTGCG-3’.

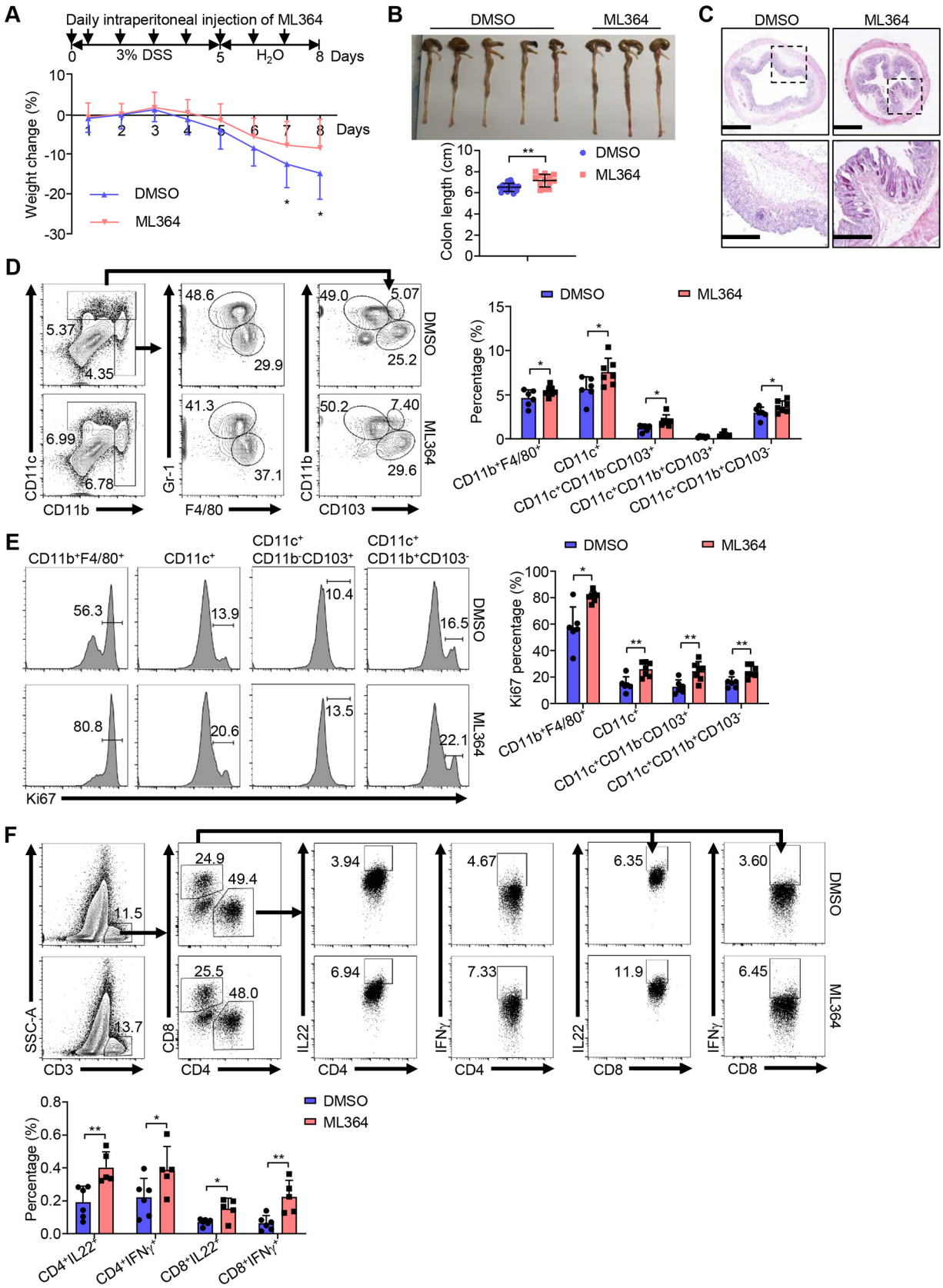

(caption on next page)

Fig. 6. Pharmacological inhibition of USP2 inhibits DSS-induced colitis.
(A) A scheme of DSS and ML364 treatment, and body weight change of WT mice that were treated successively with DMSO (n = 15) or ML364 (10 mg/kg, n = 13) for 8 days with DSS-induced colitis.
(B) The representative image and lengths of colons of WT mice treated as in (A).
(C) HE-stained images of colon sections of WT mice treated as in (A).
(D) Flow cytometry analysis and proportions of $CD11b^{+}F4/80^{+}$ macrophages, $CD11c^{+}$, $CD11c^{+}CD11b^{-}CD103^{+}$, $CD11c^{+}CD11b^{+}CD103^{+}$ and $CD11c^{+}CD11b^{+}CD103^{-}$ DCs in LPMCs from WT mice that were treated successively with DMSO (n = 6) or ML364 (10 mg/kg, n = 7) for 8 days with DSS-induced colitis.
(E) Flow cytometry analysis and proportions of Ki67 in $CD11b^{+}F4/80^{+}$ macrophages, $CD11b^{-}CD103^{+}$, $CD11b^{+}CD103^{+}$, $CD11b^{+}CD103^{-}$ DCs of LPMCs from WT mice that were treated successively with DMSO (n = 6) or ML364 (10 mg/kg, n = 7) for 8 days with DSS-induced colitis.
(F) Flow cytometry analysis and proportions of IL-22- and IFNγ-producing T lymphocytes in LPMCs from WT mice that were treated successively with DMSO (n = 6) or ML364 (10 mg/kg, n = 5) for 8 days with DSS-induced colitis.
$^{*}P < 0.05$, $^{**}P < 0.01$, $^{***}P < 0.001$ (Student's unpaired *t*-test). Scale bars represent 600 μm, 200 μm. Graphs show mean ± S.D. (A-B, D-F). Data are a combination of three (A–C) or two (D–F) independent experiments.

4.2. DSS-induced colitis models

Eight-week-old mice were given 3% DSS (MP Biomedicals) in the drinking water (w/v) for 5 days and followed by normal drinking water for 3 days before sacrifice. Body weight, bleeding, and stool was observed and recorded daily during this period. After the mice were sacrificed, their colons and mesenteric lymph nodes were collected for various analyses.

4.3. The treatment of ML364

ML364 purchased from Selleck Chemicals was stocked as a powder at −80 °C. For treatment of mice, ML364 dissolved in DMSO was diluted in 100–200 μL of PBS and intraperitoneally injected mice (10 mg per kg body weight).

4.4. Colitis analysis

The colon tissues (from the cecum to the anus) of mice with DSS-induced colitis were measured and recorded. The distal colon tissues were fixed in 4% paraformaldehyde for 4 h and dehydrated in gradient ethanol before paraffin embedding. The paraffin tissue blocks were sectioned (6 μm) and stained with HE (Beyotime Biotech) and Masson trichrome (Leagene) for Aperio VERSA scanner (Leica) to evaluate injury and inflammation of colon and production of collagen. Pathogenic scores of inflamed colons consisted of disease activity index (DAI) score and histopathological score. DAI score as an accumulative score in the light of stool condition (score: 0, normal; 1, soft stools; 2, loose stools; 3, diarrhea), rectal bleeding (score: 0, normal; 1 and 2, bloody stools; 3, severe bleeding) and body weight loss (score: 0, none; 1, 1%–5%; 2, 5%–10%; 3, 10%–15%; 4, >15%). Histopathological score as a collective score on the grounds of epithelial damage (0, normal morphology; 1, loss of goblet cells; 2, loss of more than half of the goblet cells; 3, loss of crypts; 4, loss of more than half of the crypts) and inflammatory cell infiltration (0, no infiltration; 1, infiltrating crypt bases; 2, infiltrating muscularis mucosa; 3, infiltrating the muscularis mucosa with abundant edema; 4, infiltrating submucosa). The pathogenic scores of inflamed colons were scored without any previous knowledge of the experimental groups.

4.5. Isolation of colon cells

Colons were removed and put in pre-cooled PBS. Subsequently, colons were opened longitudinally and cut into about 1 cm pieces. These pieces were transferred to 5 mL RPMI 1640 medium including 1 mM DTT, 5 mM EDTA, 20 mM HEPES, and 1 × Penicillin-Streptomycin Solution, and shook for 30 min at 37 °C to dissociate the epithelial cell. The digested pieces of colons were washed twice with PBS and placed in 5 mL RPMI 1640 medium containing 50 μg/mL DNase I, 1.5 mg/mL collagenase D, 20 mM HEPES and 1 × Penicillin-Streptomycin Solution to shake for 30 min at 37 °C. The cells from digested colons were obtained by filtrating and centrifuging at 2000 r.p.m for 10 min. Cell precipitates were resuspended with 4 mL 40% Percoll to be cell suspension, which was covered 4 mL 80% Percoll and then centrifuged for 30 min at 2000 r.p.m at room temperature. lamina propria mononuclear lymphocytes were collected from the white interface in the middle of the Percoll gradient by centrifuging at 2000 r.p.m for 5 min. The lamina propria mononuclear lymphocytes were sorted by a positive selection kit (Invitrogen) to obtain the $CD4^{+}$ cells.

4.6. Flow cytometry analysis and sorting

Cells derived from lamina propria or mesenteric lymph nodes were resuspended in PBS containing 1% FBS and blocked with anti-CD16/32 antibodies according to 1:200 at 4 °C for 10 min. Subsequently, cells were stained with specific antibodies for flow cytometry analysis. For cell surface staining, the cells were incubated with antibodies at 4 °C in dark for 15 min. For intracellular marker staining, cells were fixed and permeabilized with the Fixation/Permeabilization Buffer (BioLegend) according to the manufacturer's instructions after they have been stained for cell-surface markers. The following fluorescence-labeled antibodies were used: anti-CD16/32 (Biolegend, 101302), anti-CD11b-FITC (101206), anti-CD11b-PE (101207), anti-CD11c-PerCP/Cy5.5 (117327), anti-CD11c-APC (117309), anti-CD11c-PE (117307), anti-F4/80-PE (123110), anti-Gr-1-APC (108411), anti-Ly-6G-APC/Cy7 (127623), anti-MHCII-APC (107613), anti-MHCII-BV421 (107631), anti-CD86-FITC (Sungene Biotech, M10034-02B), anti-CD80-FITC (104705), anti-CD103- PE-CF594 (121429), anti-CD3-PE (100308), anti-CD4-FITC (100406), anti-CD8-BV510 (100751), anti-CD19-APC (M10191-11c), anti-CD25-PerCP (M10251-32A), anti-CD62L-APC (104411), anti-CD44-PE (103007), anti-IL17A-BV421 (506925), anti-–IFNγ-PerCP/Cy5.5 (505822), anti-FoxP3-APC (Invitrogen, 17-5773-80), anti-IL22-APC (Bioss, bs-2623R-APC), anti-Ki67-PerCP-eFluor710 (Invitrogen, 46-5698-82), anti-p-p65 (Ser468)-APC (bs-3485R-APC) and anti-p-SMAD2 (Ser465)-APC (bs-2224R-APC). For intracellular staining of cytokines (IL17A, IL22, IFNγ), cells were cultured with PMA (50 ng/mL), ionomycin (500 ng/mL), and GolgiStop (1:1000, BD Biosciences) in RPMI 1640 medium at 37 °C for 4.5 h to stimulate cytokine production before staining. For cell sorting, cells from lamina propria were sorted by $CD45^{+}$ positive selection kit (BioLegend) previously and sorted by Flow cytometry (BD FACSAria II) to obtain highly purified target cells.

4.7. mRNA-sequencing analysis

Target cells obtained by sorting lamina propria cells from inflamed colons were lysed in 500 μL of TRIzol (Invitrogen). Total RNAs were prepared and the quality of RNAs was determined by agarose gel electrophoresis and spectrophotometer analysis. Poly (A) mRNA was enriched from at least 1 μg total RNA by Oligo (dT) using NEBNext Ultra II RNA Library Prep Kit for Illumina and interrupted randomly by divalent cations. cDNA was synthesized using the fragmented mRNAs as templates and random oligodeoxynucleotides as primers. The double-stranded cDNA was purified followed by repairing the double end and introducing base "A" at 3′ end and connecting sequencing adapters. About 400–500 bp cDNA was screened by AMPure XP beads and

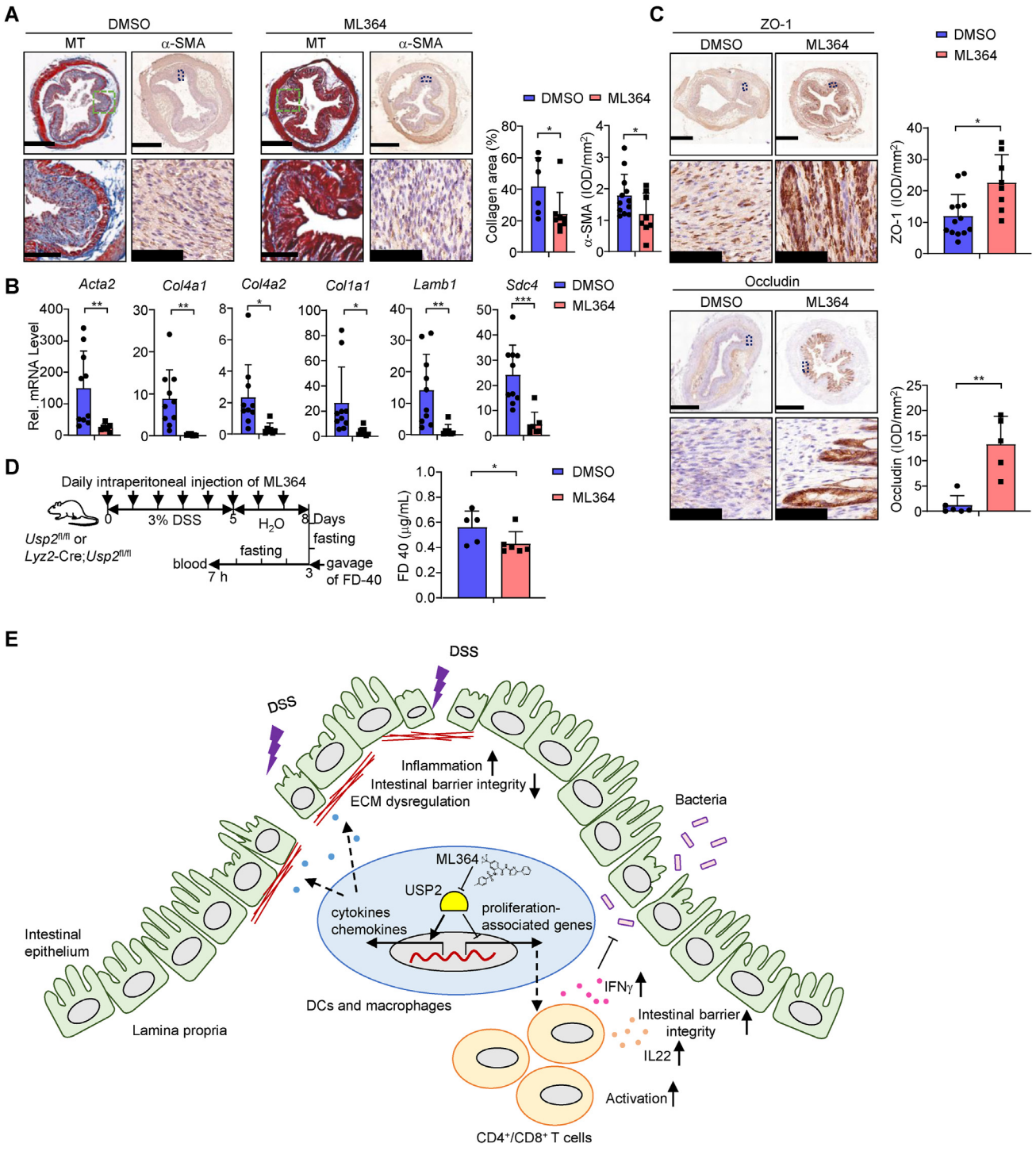

Fig. 7. Pharmacological inhibition of USP2 inhibits ECM dysregulation in DSS-induced colitis.

(A) Masson staining and anti-α-SMA immunohistochemistry staining, the percentage of collagen-positive areas and the IOD per mm^2 analysis of α-SMA in colon sections of WT mice that were treated successively with DMSO (n = 6; 12) or ML364 (10 mg/kg, n = 8; 8) for 8 days with DSS-induced colitis.

(B) qRT-PCR results of ECM-related genes in colon tissues from WT mice treated successively with DMSO (n = 10) or ML364 (10 mg/kg, n = 7) for 8 days with DSS-induced colitis.

(C) Anti-ZO-1 and anti-Occludin immunohistochemistry staining, the integral optical density (IOD) per mm^2 analysis of ZO-1 and Occludin in colon sections of WT mice that were treated successively with DMSO (n = 13; 6) or ML364 (10 mg/kg, n = 8; 5) for 8 days with DSS-induced colitis.

(D) Schematic illustration and the concentration of FD-40 in peripheral blood of posterior orbital venous plexus from WT mice that were treated successively with DMSO (n = 5) or ML364 (10 mg/kg, n = 6) for 8 days with DSS-induced colitis.

(E) A model for USP2 to modulate colonic infections and inflammations. USP2 inhibits the proliferation of macrophages and DCs to suppress T cells activation, which leads to the inhibition of repair and the susceptibility of bacteria, and promotes the production of cytokines and chemokines to dysregulate ECM, destroying the integrity of intestinal barrier, aggravating DSS-induced colitis. Pharmacologically inhibition of USP2 alleviates DSS-induced colitis.

$^*P < 0.05$, $^{**}P < 0.01$, $^{***}P < 0.001$ (Student's unpaired *t*-test). Scale bars represent 600 μm, 200 μm and 100 μm. Graphs show mean ± S.D. (A–D). Data are a combination of two (A–C) independent experiments or representative of two (D) independent experiments.

amplified using PCR. The PCR products were purified by AMPure XP Beads and libraries were obtained. After testing the quality, libraries were sequenced on the Illumina NovaSeq 6000 platform with Illumina HiSeq PE 150 strategy (Personalbio). Quality control of mRNA-seq data was performed by FastQc (v 0.11.8) and adapter bases placed in 3' end were trimmed by Cutadapt (v 1.1.5). All RNA-seq data were mapped to the mouse genome (GRCm39) by HISAT2 (v 2.0.5) and allowed a maximum of two mismatches per read. Gene expression level was calculated by HTSeq (v 0.9.1) with default parameters and normalized by FPKM.

4.8. Bacterial infection

Citrobacter rodentium (ICC168) was described previously (Li et al., 2013a) and kindly provided by S. Li (Huazhong Agricultural University). Mice were injected by gavage with approximately 1×10^9 c.f.u. of *Citrobacter rodentium* suspended in 200 μL of sterile PBS. The weight of mice was monitored daily. At indicated time points after infection, mice were killed and the colon was removed for analysis. For analysis of fecal bacteria count, fresh feces were collected and dissolved in sterile PBS, which was serially diluted and plated on conditional LB agar plates. The bacterial colonies were counted after incubation at 37 °C for 12 h.

4.9. qRT-PCR

Total RNA was extracted from cells using 500 μL TRIzol (Invitrogen), and the first strand of cDNA was reverse transcribed using All-in-One cDNA Synthesis SuperMix (Biotool). Gene expression was examined by the fast two-step amplification program using 2 × SYBR Green Fast qRT-PCR Master Mix (Biotool) on the BioRad CFX Connect system. The value obtained from each gene was normalized to that of the gene encoding β-actin. The sequences of primers involved in this study were listed in Table S1.

4.10. Immunohistochemistry

Paraffin sections of colon tissues were dewaxed in xylene followed by hydration in gradient ethanol. Antigen retrieval was performed by heating slides in a microwave for 40 min in sodium citrate buffer (pH 6.0). Then the slides were cooled down naturally to room temperature before being quenched in 3% hydrogen peroxide to block endogenous peroxidase activity. The primary antibody diluted in PBS containing 1% BSA (α-SMA, 1:500; ZO-1, 1:400, Occludin, 1:200) was incubated at 4 °C overnight followed by General purpose SP Kit (ZSGB-Bio) and DAB immunochromogenic reagent (Gene Tech) according to the manufacturer's instructions. Subsequently, the slides were counterstained with hematoxylin (Beyotime Biotech) for 15 s and cover slipped. Images were acquired with Aperio VERSA scanner (Leica). The intensities of DAB staining were measured and quantified with integrated optical density or cell intensity by Image Pro Plus 6 (Media Cybernetics). The following immunohistochemical antibodies were used: α-SMA (Sigma, A2547); ZO-1(Bioss, bs-1329R); Occludin (Abcam, ab216327).

4.11. Colon organoid culture

The colons from eight-week-old healthy mice were cut into small pieces and digested in pre-cooled PBS containing 2 mM EDTA and 1 × Penicillin-Streptomycin Solution with shaking for 1 h at 4 °C to dissociate epithelial cells. Pipet the colon pieces up and down softly and centrifuge to collect crypts. Construct the three-dimensional cultured model in vitro with Matrigel and IntestiCult (Mouse) medium to culture crypts for 5–6 days until organoids mature. After organoids matured, crush the Matrigel and centrifuge to collect organoids. Resuspend the organoid pellets and culture the organoids for 24 h at 37 °C with the conditional medium that is a mixture of complete DMEM medium and culture medium of target cells according to the ratio of 1:1.

4.12. FITC-dextran assay in vivo

The mice with DSS-induced colitis were fasted for 3 h and then gavaged with FITC-dextran (aladdin, F291057) dissolved in sterile water at a dose of 40 mg per 100 g body weight. After 4 h, blood was taken from the posterior orbital venous plexus, and the serum was isolated by centrifugation at 3000×*g* for 10 min at 4 °C. To measure the serum absorbance of FD-40, a fluorescence microplate reader was used with an excitation wavelength of 488 nm and emission wavelength of 525 nm.

4.13. TGF-β stimulation in vitro

The cells were placed in 48-well plates with a density of 1–2 × 10^5 cells per well and cultured in RPMI 1640 medium at 37 °C. TGF-β (Peprotech, 100-21C) was dissolved in 0.1% BSA and stimulated cells at a concentration of 10 ng/mL at 37 °C.

Ethics statement

All mice were housed in the specific pathogen-free facility, and DSS-induced colitis experiments and *Citrobacter rodentium* infection experiments were carried out in an SPF and ABSL-2 facility at the Medical Research Institute of Wuhan University. The experimental protocol has adhered to the International Guiding Principles for Biomedical Involving Animals. The protocol for animal experiments was approved by the Institutional Animal Care and Use Committee of the Medical Research Institute of Wuhan University (approval number S10221020A).

Statistical analysis

Differences between experimental and control groups were tested using the Unpaired or Paired Student's *t*-test. *P* values less than 0.05 were considered statistically significant.

Author contributions

B.Z. and Z.D.Z. supervised the study. R.A. performed the major experiments. P.W. helped with mouse breeding and genotyping. H.G. helped with DSS-induced colitis modeling. B.Z., Z.D.Z., and R.A. wrote the paper. All the authors analyzed data.

Conflict of interest

The authors declare no conflict of interest.

Acknowledgments

The authors thank Drs. Yan Zhou (Wuhan University) and Xin-Dong Liu (Army Medical University) for mice on this study, Drs. Shan Li (Huazhong Agricultural University) and Hao-Jian Zhang (Wuhan University) for reagents and technical support, members of the Zhong laboratory and the core facilities of the Medical Research Institute for technical support. This study was supported by grants from the National Key Research and Development Program of China (Grant Nos. 2018TFE0204500 and 2018YFC1004601), Natural Science Foundation of China (Grant Nos. 31930040 and 32000636), Natural Science Foundation of Hubei Province (Grant No. 2020CFA015), Fundamental Research Funds for Central Universities (Grant Nos. 2042022kf1187, 2042020kf0042, and 2042022kf1123), and the Non-Profit Central Research Institute Fund of Chinese Academy of Medical Sciences (Grant No. 2020PT320-004).

Appendix A. Supplementary data

Supplementary data to this article can be found online at https://doi.org/10.1016/j.cellin.2022.100047.

References

Akira, S., Uematsu, S., & Takeuchi, O. (2006). Pathogen recognition and innate immunity. *Cell, 124*, 783–801.

Ananthakrishnan, A. N., Bernstein, C. N., Iliopoulos, D., Macpherson, A., Neurath, M. F., Ali, R. A. R., Vavricka, S. R., & Fiocchi, C. (2018). Environmental triggers in IBD: a review of progress and evidence. *Nat. Rev. Gastroenterol. Hepatol., 15*, 39–49.

Andres, V., Pello, O. M., & Silvestre-Roig, C. (2012). Macrophage proliferation and apoptosis in atherosclerosis. *Curr. Opin. Lipidol., 23*, 429–438.

Bassler, K., Schulte-Schrepping, J., Warnat-Herresthal, S., Aschenbrenner, A. C., & Schultze, J. L. (2019). The myeloid cell compartment-cell by cell. *Annu. Rev. Immunol., 37*, 269–293.

Bataller, A., Montalban-Bravo, G., Soltysiak, K. A., & Garcia-Manero, G. (2019). The role of TGFbeta in hematopoiesis and myeloid disorders. *Leukemia, 33*, 1076–1089.

Ben-Sasson, S. Z., Hu-Li, J., Quiel, J., Cauchetaux, S., Ratner, M., Shapira, I., Dinarello, C. A., & Paul, W. E. (2009). IL-1 acts directly on CD4 T cells to enhance their antigen-driven expansion and differentiation. *Proc. Natl. Acad. Sci. U. S. A., 106*, 7119–7124.

Billiau, A., & Matthys, P. (2009). *Interferon-gamma: a Historical Perspective* (pp. 97–113). Cytokine Growth Factor Rev 20.

Bonnans, C., Chou, J., & Werb, Z. (2014). Remodelling the extracellular matrix in development and disease. *Nat. Rev. Mol. Cell Biol., 15*, 786–801.

Cleynen, I., Boucher, G., Jostins, L., Schumm, L. P., Zeissig, S., Ahmad, T., Andersen, V., Andrews, J. M., Annese, V., Brand, S., et al. (2016). Inherited determinants of Crohn's disease and ulcerative colitis phenotypes: a genetic association study. *Lancet, 387*, 156–167.

Gerner, M. Y., Heltemes-Harris, L. M., Fife, B. T., & Mescher, M. F. (2013). Cutting edge: IL-12 and type I IFN differentially program CD8 T cells for programmed death 1 re-expression levels and tumor control. *J. Immunol., 191*, 1011–1015.

Glocker, E. O., Kotlarz, D., Boztug, K., Gertz, E. M., Schaffer, A. A., Noyan, F., Perro, M., Diestelhorst, J., Allroth, A., Murugan, D., et al. (2009). Inflammatory bowel disease and mutations affecting the interleukin-10 receptor. *N. Engl. J. Med., 361*, 2033–2045.

Gunzel, D., & Yu, A. S. (2013). Claudins and the modulation of tight junction permeability. *Physiol. Rev., 93*, 525–569.

Huang, L., Li, G. H., Yu, Q., Xu, Y., Cvetkovski, S., Wang, X., Parajuli, N., Udo-Inyang, I., Kaplan, D., Zhou, L., et al. (2020). Smad2/4 signaling pathway is critical for epidermal langerhans cell repopulation under inflammatory condition but not required for their homeostasis at steady state. *Front. Immunol., 11*, 912.

Hulsmans, M., Sam, F., & Nahrendorf, M. (2016). Monocyte and macrophage contributions to cardiac remodeling. *J. Mol. Cell. Cardiol., 93*, 149–155.

Karki, R., Man, S. M., & Kanneganti, T. D. (2017). Inflammasomes and cancer. *Cancer Immunol Res, 5*, 94–99.

Kim, J., Kim, W. J., Liu, Z., Loda, M., & Freeman, M. R. (2012). The ubiquitin-specific protease USP2a enhances tumor progression by targeting cyclin A1 in bladder cancer. *Cell Cycle, 11*, 1123–1130.

Kitamura, H., & Hashimoto, M. (2021). USP2-Related cellular signaling and consequent pathophysiological outcomes. *Int. J. Mol. Sci., 22*.

Lautenschlager, F., Paschke, S., Schinkinger, S., Bruel, A., Beil, M., & Guck, J. (2009). The regulatory role of cell mechanics for migration of differentiating myeloid cells. *Proc. Natl. Acad. Sci. U. S. A., 106*, 15696–15701.

Lawrance, I. C., Rogler, G., Bamias, G., Breynaert, C., Florholmen, J., Pellino, G., Reif, S., Speca, S., & Latella, G. (2017). Cellular and molecular mediators of intestinal fibrosis. *J Crohns Colitis, 11*, 1491–1503.

Li, H., Qi, Y., & Jasper, H. (2016). Preventing age-related decline of gut compartmentalization limits microbiota dysbiosis and extends lifespan. *Cell Host Microbe, 19*, 240–253.

Li, S., Zhang, L., Yao, Q., Li, L., Dong, N., Rong, J., Gao, W., Ding, X., Sun, L., Chen, X., et al. (2013a). Pathogen blocks host death receptor signalling by arginine GlcNAcylation of death domains. *Nature, 501*, 242–246.

Li, W., Shen, W., Zhang, B., Tian, K., Li, Y., Mu, L., Luo, Z., Zhong, X., Wu, X., Liu, Y., et al. (2020). Long non-coding RNA LncKdm2b regulates cortical neuronal differentiation by cis-activating Kdm2b. *Protein Cell, 11*, 161–186.

Li, Y., He, X., Wang, S., Shu, H. B., & Liu, Y. (2013b). USP2a positively regulates TCR-induced NF-kappaB activation by bridging MALT1-TRAF6. *Protein Cell, 4*, 62–70.

Liuyu, T., Yu, K., Ye, L., Zhang, Z., Zhang, M., Ren, Y., Cai, Z., Zhu, Q., Lin, D., & Zhong, B. (2019). Induction of OTUD4 by viral infection promotes antiviral responses through deubiquitinating and stabilizing MAVS. *Cell Res., 29*, 67–79.

Mencarelli, A., Khameneh, H. J., Fric, J., Vacca, M., El Daker, S., Janela, B., Tang, J. P., Nabti, S., Balachander, A., Lim, T. S., et al. (2018). Calcineurin-mediated IL-2 production by CD11c(high)MHCII(+) myeloid cells is crucial for intestinal immune homeostasis. *Nat. Commun., 9*, 1102.

Meng, X., Vander Ark, A., Lee, P., Hostetter, G., Bhowmick, N. A., Matrisian, L. M., Williams, B. O., Miranti, C. K., & Li, X. (2016). Myeloid-specific TGF-beta signaling in bone promotes basic-FGF and breast cancer bone metastasis. *Oncogene, 35*, 2370–2378.

Meng, X., Xiong, Z., Xiao, W., Yuan, C., Wang, C., Huang, Y., Tong, J., Shi, J., Chen, Z., Liu, C., et al. (2020). Downregulation of ubiquitin-specific protease 2 possesses prognostic and diagnostic value and promotes the clear cell renal cell carcinoma progression. *Ann. Transl. Med., 8*, 319.

Neurath, M. F. (2019). Targeting immune cell circuits and trafficking in inflammatory bowel disease. *Nat. Immunol., 20*, 970–979.

Oami, T., & Coopersmith, C. M. (2021). Measurement of intestinal permeability during sepsis. *Methods Mol. Biol., 2321*, 169–175.

Ogle, M. E., Segar, C. E., Sridhar, S., & Botchwey, E. A. (2016). Monocytes and macrophages in tissue repair: implications for immunoregenerative biomaterial design. *Exp. Biol. Med., 241*, 1084–1097.

Ogura, Y., Bonen, D. K., Inohara, N., Nicolae, D. L., Chen, F. F., Ramos, R., Britton, H., Moran, T., Karaliuskas, R., Duerr, R. H., et al. (2001). A frameshift mutation in NOD2 associated with susceptibility to Crohn's disease. *Nature, 411*, 603–606.

Pugliese, D., Felice, C., Papa, A., Gasbarrini, A., Rapaccini, G. L., Guidi, L., & Armuzzi, A. (2017). Anti TNF-alpha therapy for ulcerative colitis: current status and prospects for the future. *Expet Rev. Clin. Immunol., 13*, 223–233.

Quiros, M., & Nusrat, A. (2019). Contribution of wound-associated cells and mediators in orchestrating gastrointestinal mucosal wound repair. *Annu. Rev. Physiol., 81*, 189–209.

Rathinam, V. A. K., & Chan, F. K. (2018). Inflammasome, inflammation, and tissue homeostasis. *Trends Mol. Med., 24*, 304–318.

Rieder, F., Zimmermann, E. M., Remzi, F. H., & Sandborn, W. J. (2013). Crohn's disease complicated by strictures: a systematic review. *Gut, 62*, 1072–1084.

Roche, P. A., & Furuta, K. (2015). The ins and outs of MHC class II-mediated antigen processing and presentation. *Nat. Rev. Immunol., 15*, 203–216.

Shah, R., Cope, J. L., Nagy-Szakal, D., Dowd, S., Versalovic, J., Hollister, E. B., & Kellermayer, R. (2016). Composition and function of the pediatric colonic mucosal microbiome in untreated patients with ulcerative colitis. *Gut Microb., 7*, 384–396.

Shamoon, M., Martin, N. M., & O'Brien, C. L. (2019). Recent advances in gut Microbiota mediated therapeutic targets in inflammatory bowel diseases: emerging modalities for future pharmacological implications. *Pharmacol. Res., 148*, Article 104344.

Shi, Y., Solomon, L. R., Pereda-Lopez, A., Giranda, V. L., Luo, Y., Johnson, E. F., Shoemaker, A. R., Leverson, J., & Liu, X. (2011). Ubiquitin-specific cysteine protease 2a (USP2a) regulates the stability of Aurora-A. *J. Biol. Chem., 286*, 38960–38968.

Shu, D. Y., & Lovicu, F. J. (2017). Myofibroblast transdifferentiation: the dark force in ocular wound healing and fibrosis. *Prog. Retin. Eye Res., 60*, 44–65.

Smillie, C. S., Biton, M., Ordovas-Montanes, J., Sullivan, K. M., Burgin, G., Graham, D. B., Herbst, R. H., Rogel, N., Slyper, M., Waldman, J., et al. (2019). Intra- and inter-cellular rewiring of the human colon during ulcerative colitis. *Cell, 178*, 714–730 e722.

Stevenson, L. F., Sparks, A., Allende-Vega, N., Xirodimas, D. P., Lane, D. P., & Saville, M. K. (2007). The deubiquitinating enzyme USP2a regulates the p53 pathway by targeting Mdm2. *EMBO J., 26*, 976–986.

Strober, W., Fuss, I., & Mannon, P. (2007). The fundamental basis of inflammatory bowel disease. *J. Clin. Invest., 117*, 514–521.

Sugimoto, K., Ogawa, A., Mizoguchi, E., Shimomura, Y., Andoh, A., Bhan, A. K., Blumberg, R. S., Xavier, R. J., & Mizoguchi, A. (2008). IL-22 ameliorates intestinal inflammation in a mouse model of ulcerative colitis. *J. Clin. Invest., 118*, 534–544.

Sun, Y., Qin, Z., Li, Q., Wan, J. J., Cheng, M. H., Wang, P. Y., Su, D. F., Yu, J. G., & Liu, X. (2016). MicroRNA-124 negatively regulates LPS-induced TNF-alpha production in mouse macrophages by decreasing protein stability. *Acta Pharmacol. Sin., 37*, 889–897.

Tacke, F., & Zimmermann, H. W. (2014). Macrophage heterogeneity in liver injury and fibrosis. *J. Hepatol., 60*, 1090–1096.

Thery, C., & Amigorena, S. (2001). The cell biology of antigen presentation in dendritic cells. *Curr. Opin. Immunol., 13*, 45–51.

Tsou, C. L., Peters, W., Si, Y., Slaymaker, S., Aslanian, A. M., Weisberg, S. P., Mack, M., & Charo, I. F. (2007). Critical roles for CCR2 and MCP-3 in monocyte mobilization from bone marrow and recruitment to inflammatory sites. *J. Clin. Invest., 117*, 902–909.

Tu, Y., Xu, L., Xu, J., Bao, Z., Tian, W., Ye, Y., Sun, G., Miao, Z., Chao, H., You, Y., et al. (2022). Loss of deubiquitylase USP2 triggers development of glioblastoma via TGF-beta signaling. *Oncogene, 41*, 2597–2608.

van Amerongen, M. J., Harmsen, M. C., van Rooijen, N., Petersen, A. H., & van Luyn, M. J. (2007). Macrophage depletion impairs wound healing and increases left ventricular remodeling after myocardial injury in mice. *Am. J. Pathol., 170*, 818–829.

Wang, J., Lin, S., Brown, J. M., van Wagoner, D., Fiocchi, C., & Rieder, F. (2021). Novel mechanisms and clinical trial endpoints in intestinal fibrosis. *Immunol. Rev., 302*, 211–227.

Wang, X. M., Yang, C., Zhao, Y., Xu, Z. G., Yang, W., Wang, P., Lin, D., Xiong, B., Fang, J. Y., Dong, C., et al. (2020). The deubiquitinase USP25 supports colonic inflammation and bacterial infection and promotes colorectal cancer. *Nat. Can. (Que.), 1*, 811–825.

Wen, Y., Yan, H. R., Wang, B., & Liu, B. C. (2021). Macrophage heterogeneity in kidney injury and fibrosis. *Front. Immunol., 12*, Article 681748.

Wu, X., Wang, Y., Huang, R., Gai, Q., Liu, H., Shi, M., Zhang, X., Zuo, Y., Chen, L., Zhao, Q., et al. (2020). SOSTDC1-producing follicular helper T cells promote regulatory follicular T cell differentiation. *Science, 369*, 984–988.

Xavier, R. J., & Podolsky, D. K. (2007). Unravelling the pathogenesis of inflammatory bowel disease. *Nature, 448*, 427–434.

Xu, Q., Liu, M., Zhang, F., Liu, X., Ling, S., Chen, X., Gu, J., Ou, W., Liu, S., & Liu, N. (2021). Ubiquitin-specific protease 2 regulates Ang -induced cardiac fibroblasts activation by up-regulating cyclin D1 and stabilizing beta-catenin in vitro. *J. Cell Mol. Med., 25*, 1001–1011.

Yamazaki, K., McGovern, D., Ragoussis, J., Paolucci, M., Butler, H., Jewell, D., Cardon, L., Takazoe, M., Tanaka, T., Ichimori, T., et al. (2005). Single nucleotide polymorphisms in TNFSF15 confer susceptibility to Crohn's disease. *Hum. Mol. Genet., 14*, 3499–3506.

Yilmaz, B., Juillerat, P., Oyas, O., Ramon, C., Bravo, F. D., Franc, Y., Fournier, N., Michetti, P., Mueller, C., Geuking, M., et al. (2019). Microbial network disturbances in relapsing refractory Crohn's disease. *Nat Med, 25*, 323–336.

Ying, W., Fu, W., Lee, Y. S., & Olefsky, J. M. (2020). The role of macrophages in obesity-associated islet inflammation and beta-cell abnormalities. *Nat. Rev. Endocrinol., 16*, 81–90.

Zhao, Y., Wang, X., Wang, Q., Deng, Y., Li, K., Zhang, M., Zhang, Q., Zhou, J., Wang, H. Y., Bai, P., et al. (2018). USP2a supports metastasis by tuning TGF-beta signaling. *Cell Rep., 22*, 2442–2454.